Study of Lithium Ion Conducting Ga, Sr and Nb Doped $Li_7La_3Zr_2O_{12}$ Solid Electrolyte

Dissertation submitted to

Visvesvaraya National Institute of Technology, Nagpur

in partial fulfilment of the requirement for the award of

the degree

Master of Science

In

Physics

By

Priya Shivappa Padaganur

(MS23PHY011)

Under the guidance of

Dr. (Mrs.) A.V. Deshpande

Department Of Physics

Visvesvaraya National Institute of Technology Nagpur 440010 (India)

2025

Study of Lithium Ion Conducting Ga, Sr and Nb Doped $Li_7La_3Zr_2O_{12}$ Solid Electrolyte

Dissertation submitted to

Visvesvaraya National Institute of Technology, Nagpur

in partial fulfilment of the requirement for the award of

the degree

Master of Science

In

Physics

By

Priya Shivappa Padaganur

(MS23PHY011)

Under the guidance of

Dr. (Mrs.) A.V. Deshpande

Department Of Physics

Visvesvaraya National Institute of Technology Nagpur 440010 (India)

2025

© Visvesvaraya National Institute of Technology (VNIT) 2025

VISVESVARAYA NATIONAL INSTITUTE OF TECHNOLOGY, NAGPUR,

DEPARTMENT OF PHYSICS.

Dissertation approval sheet

Dissertation entitled **"Study of Lithium Ion Conducting Ga, Sr and Nb Doped $Li_7La_3Zr_2O_{12}$ Solid Electrolyte"** by Priya Shivappa Padaganur is approved for the degree of Master of Science in Physics.

(Dr. (Mrs.) A.V. Deshpande)
Supervisor

Name:
External Examiner

Name:
Chairman

Department of Physics

Visvesvaraya National Institute of Technology, Nagpur

Declaration

I, Priya Shivappa Padaganur, hereby declare that this dissertation titled **"Study of Lithium Ion Conducting Ga, Sr and Nb Doped $Li_7La_3Zr_2O_{12}$ Solid Electrolyte"** is carried out by me in the Department of Physics of Visvesvaraya National Institute of Technology, Nagpur. The work is original and has not been submitted earlier whole or in part for the award of any degree/diploma at this or any other Institution / University.

Priya Shivappa Padaganur

Date:

Certificate

This to certify that the dissertation titled **"Study of Lithium Ion Conducting Ga, Sr and Nb Doped $Li_7La_3Zr_2O_{12}$ Solid Electrolyte"** is submitted by Priya Shivappa Padaganur in partial fulfilment of the requirements for the award of the degree of Master of Science in Physics, VNIT Nagpur. The work is comprehensive, complete and fit for final evaluation.

Dr. (Mrs.) A. V. Deshpande

Professor, Physics Department, VNIT, Nagpur

Head, Department of physics

VNIT Nagpur

Date:

Visvesvaraya National Institute of Technology, Nagpur

Non-Plagiarism Certificate

Certified that M.Sc. Dissertation titled "**Study of Lithium Ion Conducting Ga, Sr and Nb Doped $Li_7La_3Zr_2O_{12}$ Solid Electrolyte"** submitted by Priya Shivappa Padaganur Enrollment No. MS23PHY011 ID No. 30210 has been checked for plagiarism using TURNITIN software and overlap is found within prescribed limits. A summary of the report is given below;

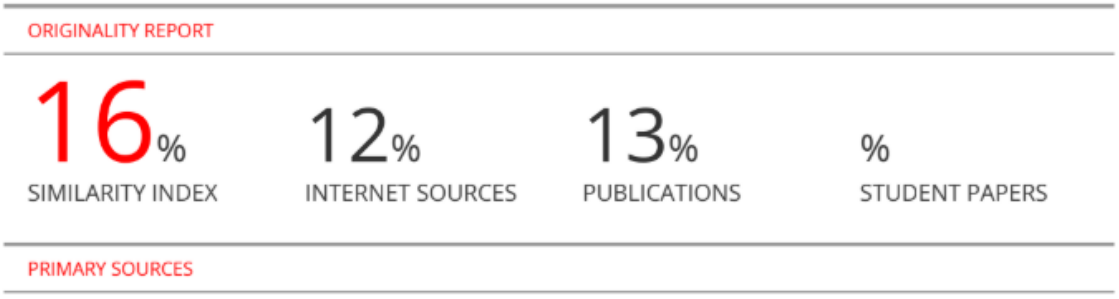

Dr. (Mrs.) A.V. Deshpande

Professor, Physics Department, VNIT, Nagpur

Priya Shivappa Padaganur

MS23PHY011

ACKNOWLEDGMENT

I would like to express my heartfelt gratitude to all those who contributed to the completion of this thesis.

First and foremost, I extend my deepest appreciation to my supervisor, Dr. (Mrs.) A.V. Deshpande, Professor of Physics Department, Visvesvaraya National Institute of Technology, Nagpur, for her invaluable guidance, unwavering support, and insightful feedback throughout the research process. Her expertise and encouragement were instrumental in shaping this work and pushing me to strive for excellence.

I am also thankful to Director, Visvesvaraya National Institute of Technology, Nagpur for providing the necessary resources and facilities that enabled me to conduct my research effectively.

I wish to convey my deep sense of gratitude to all the professors of the Physics department for their invaluable support and cooperation throughout the year. and I am also thankful to DST-FIST project (SR/FST/PSI/2017/5(C)) for the characterization.

My sincere appreciation extends to research Scholar of Physics department, Miss. Muktai M. Aote for her constructive guidance and valuable suggestions, which significantly enhanced the quality of this thesis.

I am thankful to Vaibhav. S for his contribution. Special thanks are to my friends for their encouragement, moral support, and occasional distractions that provided much-needed break during intense periods of writing and analysis.

I am indebted to my parents Mr. Shivappa. M. Padaganur and Mrs. Saroja S Padaganur and my Siblings Pooja and Venkatesh for their endless love, understanding, and encouragement. Their patience and belief in me sustained me through the challenges of this academic journey.

Thank you all for your contributions, support, and encouragement throughout this endeavour.

Priya Shivappa Padaganur

MS23PHY011

ABSTRACT

As an essential key part of solid-state lithium ion batteries, solid electrolytes are getting more attention now a days. Among all solid electrolytes, one of the most promising solid electrolyte is garnet-type $Li_7La_3Zr_2O_{12}$ (LLZO) because of its high ionic conductivity at room temperature, low activation energy, good chemical and electrochemical stability, and wide potential window. Since LLZO was first introduced, extensive research has been done in both experimental and theoretical areas. Researcher has focused on improving its performance and make LLZO a favourable solid electrolyte. These studies include developing different new methods for the synthesis of LLZO, using different crucibles and different sintering temperatures to stabilize the crystal structure, and adopting various methods of cation doping to achieve more stable LLZO with a higher ionic conductivity and lower activation energy. Here, Ga, Sr and Nb tri-doped LLZO has been prepared via solid-state reaction method, and studied as lithium ion conducting solid electrolytes. For this purpose different molar concentrations of Nb was used ranging from 0.05 to 0.15 atoms per formula unit (a.p.f.u) keeping Ga concentration fixed at 0.20 a.p.f.u and Sr concentration fixed at 0.05 a.p.f.u. Niobium substituted at the site of Zirconium leads to increased number of vacancies for lithium ion to migrate. Results showed that Ga^{3+} doping contributes to the formation of stable cubic phase at room temperature, Sr doping can give access to fine-tuning in structure and increase of Li^+ concentration. Furthermore fundamental studies were performed through X-ray diffraction, Scanning Electron Microscopy and density measurement to understand the impact of doping on LLZO crystal structure, surface morphology and on its densification respectively. The study carried out confirmed that the Ga, Sr and Nb tri-doping is beneficial for enhancing electrical properties of $Li_7La_3Zr_2O_{12}$. The optimized $Li_{6.4}Ga_{0.20}La_{2.95}Sr_{0.05}Zr_{1.95}Nb_{0.05}O_{12}$ solid electrolyte exhibits the highest ionic conductivity of 2.92 $\times 10^{-4}$ Scm^{-1} at room temperature. The variation in ionic conductivity has been corelated with the variation in relative density of the ceramics.

LIST OF FIGURES

Figure Number	TITLE	Page number
1	Types of batteries available in the market	2
2	Basic components of battery	4
3	Basic components and working principle of Li-ion cell	6
4	Crystal structure of tetragonal LLZO	11
5	Crystal structure of cubic LLZO	12
6	Experimental setup for density measurement	27
7	Sample holder for conductivity measurements	29
8	XRD pattern for Lithium lanthanum zirconium oxide	32
9	Nyquist plots at 25 ^{0}C for LLZO	33
10	Arrhenius plot of pure LLZO	34
11	X-Ray diffraction pattern of $Li_{6.45-x}Ga_{0.20}La_{2.95}Sr_{0.05}Zr_{2-x}Nb_xO_{12}$ (x= 0 to 0.15)	35
12	SEM Morphology of $Li_{6.45-x}Ga_{0.20}La_{2.95}Sr_{0.05}Zr_{2-x}Nb_xO_{12}$ [x = 0 to 0.15]	37
13	SEM of x = 0.05 and average particle size distribution for x = 0.05 The average particle size was found using SEM of x = 0.05	38
14	Elemental mapping of $Li_{6.4}Ga_{0.20}La_{2.95}Sr_{0.05}Zr_{1.95}Nb_{0.05}O_{12}$.	38
15	(a) Nyquist plots at 25°C for $Li_{6.45-x}Ga_{0.20}La_{2.95}Sr_{0.05}Zr_{2-x}Nb_xO_{12}$ (x=0 to 0.15) (b) Plot for $Li_{6.40}Ga_{0.20}La_{2.95}Sr_{0.05}Zr_{1.95}Nb_{0.05}O_{12}$ withe equivalent fitted circuit.	40
16	Conductivity as a function of temperature for $Li_{6.45-x}Ga_{0.20}La_{2.95}Sr_{0.05}Zr_{2-x}Nb_xO_{12}$ (x = 0 to 0.15)	41
17	Variation of conductivity at 25 ^{0}C and activation energy for (x= 0 to 0.15).	41
18	variation of DC conductivity with time for $Li_{6.4}Ga_{0.20}La_{2.95}Sr_{0.05}Zr_{1.95}Nb_{0.05}O_{12}$.	43

LIST OF TABLES

Table number	PARTICULARS	PAGE NUMBER
1	Chemicals used for synthesis of LLZO and its doped variant.	25
2	Density and relative density of $Li_{6.45-x}Ga_{0.20}La_{2.95}Sr_{0.05}Zr_{2-x}Nb_xO_{12}$ (x = 0 to 0.15.)	36
3	values of activation energy and conductivity varying with x in $Li_{6.45-x}Ga_{0.20}La_{2.95}Sr_{0.05}Zr_{2-x}Nb_xO_{12}$.	42

NOMENCLATURE

S/cm	Siemens per centimeter
eV	Electron volt
k	Boltzmann constant
λ	Wavelength
Å	Angstrom
mg	milligram
ρ	density
gm	gram
σ	Electrical conductivity
σ_T	Total conductivity
σ_{ion}	Ionic conductivity
$\sigma_{electron}$	Electronic conductivity
Z	Complex impedance
Zs	Real part of complex impedance
Zs”	Imaginary part of complex impedance
E_a	Activation energy

INDEX

CHAPTER NUMBER	PARTICULARS	PAGE NUMBER
CHAPTER 1	INTRODUCTION 1.1 Types of batteries 1.2 Structure of a lithium-ion battery 1.3 Working principle of a lithium-ion battery 1.4 The electrolyte 1.5 Classification of electrolytes 1.6 Types of solid electrolytes 1.7 Structure of LLZO	1-13
CHAPTER 2	REVIEW OF LITERATURE 2.1 Need of doping in LLZO 2.2 Garnet-Like Li-Ion Conductor 2.3 Single Doping 2.4 Co doping 2.5 multi doping	14-22
CHAPTER 3	SYNTHESIS AND CHARACTERIZATION 3.1 Material preparation 3.2 Characterization Techniques 3.2.1 X-ray diffraction (XRD) 3.2.2 Density 3.2.3 Scanning electron microscopy 3.2.4 Electrical conductivity Measurements 3.2.5 Impedance measurements 3.2.6 Transport Number Measurements	23-31
CHAPTER 4	RESULT AND DISCUSSION 4.1 Result and Discussion of pure LLZO 4.1.1 X-ray diffraction (LLZO) 4.1.2 Density 4.1.3 Electrical Conductivity 4.2 Result and Discussion of doped LLZO 4.2.1 X-ray diffraction 4.2.2 Density 4.2.3 Scanning electron microscopy 4.2.4 Electrical conductivity Measurements 4.2.5 Transport number measurement	32-43
CHAPTER 5	CONCLUSION 5.1Conclusions for pure LLZO 5.2 Conclusions for Ga, Sr and Nb doped LLZO 5.3 Scope for Future Work 5.4 References	44-50

CHAPTER 1
INTRODUCTION

Nations across the globe are actively pursuing sustainable energy strategies, including renewable power generation, reduction in fossil fuel dependency, enhancement of electric mobility solutions, and diverse initiatives to combat the energy challenges stemming from traditional carbon-intensive energy sources. These sustainability efforts necessitate robust energy storage mechanisms to optimize the efficiency of generated power. Consequently, improving the performance and dependability of energy conversion and storage technologies has become a critical focus area.

Prominence of Lithium Ion Technology

Among the variety storage solutions available, Li-ion battery systems have become a major technology due to their advantageous characteristics like including high energy storage capacity relative to weight, extended operational life, minimal energy loss during not actively being used working periods, and a compact design. However, these battery systems present several considerable challenges that require centralise attention from the scientific and engineering communities.

Technical and Practical Limitations

Li-ion energy storage devices face various challenges during daily use.

- Safety Considerations: They are susceptible to thermal management difficulties and risks of fire or thermal runaway increment can occur if the storage is get harmed or charged improperly.
- Degradation Over Time: The energy storage performance decreases gradually with each successive charge and discharge cycle. This corrupt of performance is due to the gradual buildup of an SEI layer resulting from continual use.
- Storage Capacity Constraints: Current energy storage systems have a restricted capacity, necessitating regular recharging to maintain optimal functionality.
- Ecological Footprint: Tracasserie at the end of a battery life cycle may discharge risky materials, negatively lashing surrounding weather.

Scientists and engineers from various countries are working hard to solve these challenges and reform the performance and dependability of lithium ion batteries.

1.1 TYPES OF BATTERIES

Energy storage market is available in different types of batteries that are designed to different uses and possess unique characteristics.

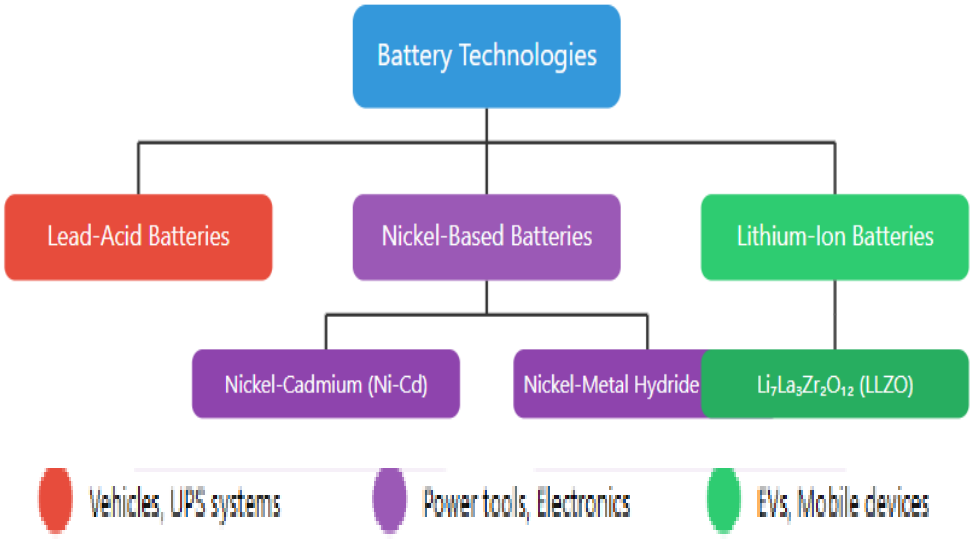

Fig 1:Types of batteries available in the market

1.1.1 Traditional Lead-Acid Systems

These well established energy storage units have become standard for automotive systems, backup power supplies and industrial application because of their dependability and cost effectiveness. Despite their extensive use in automotive and backup power application, these systems have a number of drawbacks such as substantial weight, reduced operational longevity.

1.1.2 Nickel-Cadmium Technology

The technology excels in sustaining extensive charge and discharge cycles.
Notable strengths include:

- The battery remains reliable despite exposure to various difficult situations and different temperatures.
- Rapid charging capability relative to alternative technologies.
- Suitability for high-demand applications requiring instantaneous power delivery such as electric tools.

  However, there are significant drawbacks exist:

- Likely to forget prior usage due to memory effect, where the capacity reduces with partial discharge before recharging.

- Releases cadmium which is a highly toxic substance and dangerous to the environment, and thus strict disposal measures are enforced.

- Due to dangers related to cadmium, it has been prohibited for public use in a lot of areas.

- Alongside the reduced energy storage capacity, the option is less favourable compared to more modern choices like nickel-metal hydride and lithium[1].

1.1.3 Nickel-Metal Hydride Solutions

These systems are an improvement of nickel-cadmium technology because they provide greater capacity and less environmental impact. Uses include electric vehicles, renewable energy storage, and everything in between. Some notable limitations are:

- They need to be recharged more often due to accelerated self-discharge characteristics during storage.

- They have a lower cycle life compared to lithium-based alternatives.

- They take longer than lithium-ion technology to recharge[2].

1.1.4 Lithium Ion Technology

The form factor and power capacity of Li-ion energy storage systems makes them revolutionize numerous sectors. Electric transportation vehicles, portable electronics, and even green energy storage plants predominantly rely on these power cells. The adoption of Li-ion energy storage cells stems from extended operational lifespan,

minimal upkeep, and superior performance compared to alternatives. Ongoing refinements have also resulted in improved thermal management features along with more advanced chemicals for the conductive medium. Furthermore, Li-ion energy storage technology is being further augmented into other applications due to its remarkable popularity and versatility. The technology also ensures low energy loss during idle periods, making the components indispensable for our mobile and sustainable technologies[3].

1.2 Structure of Battery

A detailed examination of battery design reveals a sophisticated system of interdependent components that cooperate to store and transmit electrical energy. These crucial structural components are described in the following section.

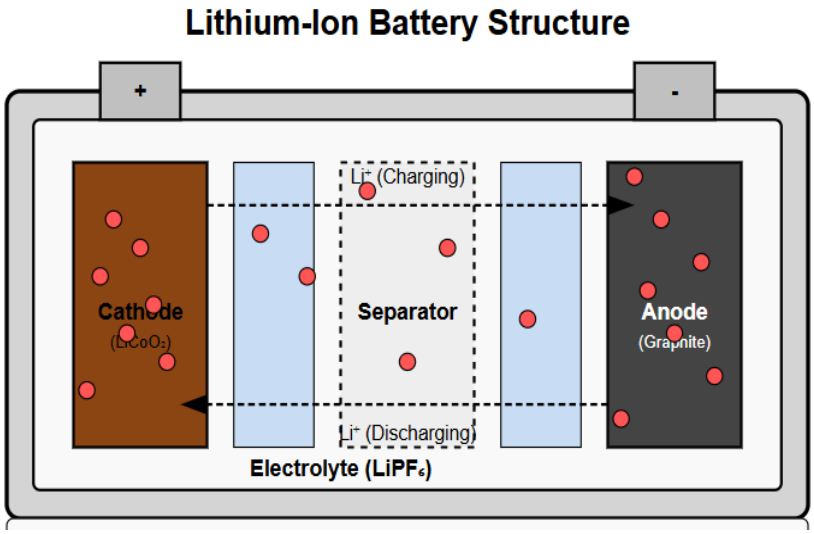

Fig 2: Basic components of battery

Negative Terminal (Anode): The negative terminal, also known as the anode, is where chemical reactions happen that release electrons. These electrons then flow out through the external circuit, creating an electric current.

Positive Terminal (Cathode): The positive terminal, also known as the cathode, is where chemical reactions happen that absorb electrons. These electrons flow back into the terminal from the external circuit, completing the circuit.

Ion Transport Medium (Electrolyte): In order to support the continuous electrochemical reaction sequence, it serves as the essential ionic conductor that permits charged particles to move between terminal electrodes.

Insulating Barrier (Separator): In order to prevent short circuits, the insulating barrier (separator) maintains selective permeability for ion transmission while providing the necessary physical isolation between opposing electrodes.

Electron Collection System: By serving as electrical current collection points, these metallic sheets direct power from electrode surfaces into an external circuit. These conductive layers, which are typically made of copper for negative terminal applications and aluminium for cathode, are essential components of the entire power transfer system.

Protective Enclosure: The outer layer that holds everything together and ensuring stability, safety, and longevity in a variety of situations.

1.3 Mechanism Behind Li-ion Battery Functionality

Fundamentally, the ability of batteries to convert chemical energy into electrical energy depends on complex electrochemical processes. These reactions function in both directions in rechargeable systems like Li-ion batteries, enabling multiple power cycles over the battery's lifespan. The operational efficiency and durability of these energy storage devices are influenced by various external and internal factors, including thermal conditions, charge rate parameters, and structural changes within component materials.

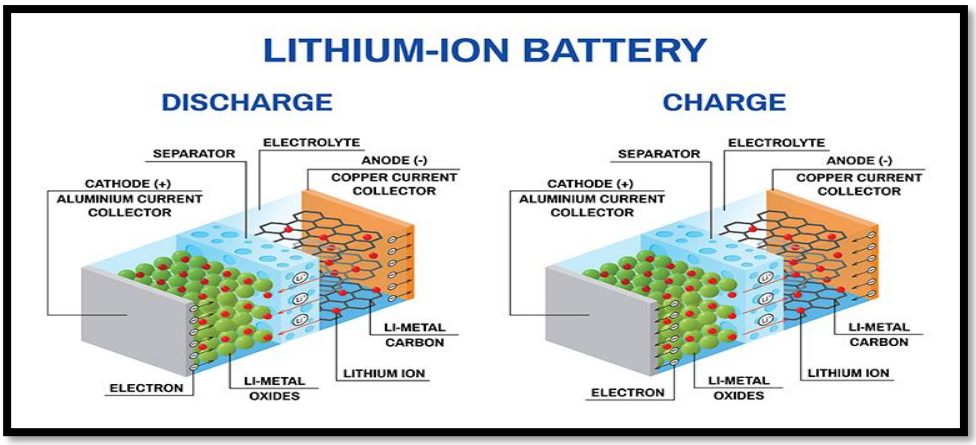

Fig 3: Basic components and working principle of lithium ion cell

Energy Storage Mechanism

When a battery connects to a power supply, the charging sequence initiates. As illustrated in Figure 3, this process drives electrons toward the cathode, while simultaneously prompting lithium or equivalent ions to traverse the electrolyte medium from the positive electrode (cathode) toward the anode. This ionic migration results in energy accumulation within the electrode materials in chemical form. The battery reaches full capacity when its voltage peaks, signaling readiness for operational.

Energy Release Mechanism

During the utilization phase, the chemically stored energy transforms into electrical current to power connected devices. As depicted in Figure 3, electrons circulate from the cathode through the external circuit to the anode, generating usable electricity. Concurrently, lithium or equivalent ions travel in the reverse direction from anode to cathode through the electrolyte solution to maintain electrical neutrality. As this discharge continues, the battery's voltage gradually diminishes until reaching a minimum threshold that necessitates recharging.

1.4 Electrolyte Functionality in Battery Systems

The electrolyte component of lithium ion batteries acts as a vital conduit for ionic flow between electrodes, promoting effective energy storage and retrieval procedures.

1.4.1 Essential functions of electrolyte in energy storage systems:

- **Ionic Conductivity:** During operating cycles, the electrolyte facilitates the migration of lithium ions between electrodes, guaranteeing efficient energy conversion and storage systems.
- **Electrical Transmission:** Electrolytes enable batteries to function with low internal resistance by preserving electrical insulation between electrodes and creating an ionically conductive environment.
- **Electrode Interface Protection:** High-quality electrolytes help to create and preserve stable boundaries between the electrolyte and electrode surfaces, reducing unwanted chemical interactions that can impair performance.
- **Safety Enhancement:** By drastically lowering the risks associated with combustibility, electrolyte seepage, and thermal instability events, modern electrolyte formulations especially solid-state variants improve operational reliability.
- **Capacity Optimization:** Advanced electrolytes significantly aid in reaching higher energy densities in modern battery designs by being compatible with high-capacity electrode materials, such as metallic lithium anodes.

1.5 Electrolyte Classification Framework

Battery electrolytes can be systematically categorized according to their fundamental physical characteristics, with distinct variations in performance attributes across different types.

Liquid-Phase Electrolyte Systems

Lithium-based salt compounds dissolved in organic solvent matrices make up the majority of liquid electrolyte formulations used in modern lithium ion energy storage devices. As the main solvent components, these usually consist of ethylene carbonate (EC), dimethyl carbonate (DMC), and diethyl carbonate (DEC).

The main benefit of fluid-state electrolytes is their remarkable ionic conductivity characteristics, which allow for quick ion migration and optimal battery performance.

Nevertheless, these systems pose serious operational risks, such as chemical degradation pathways, containment failures, and possible combustibility[4].

Adding specialized chemical additives, especially fluorinated compounds, is a common performance enhancement strategy that significantly improves electrochemical stability parameters and overall device performance metrics[5].

Solid-State Electrolyte Technologies

By completely avoiding liquid components, solid electrolyte materials offer a novel solution to many of the drawbacks of traditional electrolyte systems. For advanced energy storage applications especially next-generation lithium ion architectures this revolutionary material class offers ground-breaking enhancements in operational safety margins, service lifespan, and thermal resistance characteristics.

Solid state alternatives offer a significantly higher reliability viewpoint than conventional fluid-based electrolyte systems, which are inherently susceptible to leakage, ignition, and chemical breakdown[6].

Comparative Advantages of Solid Electrolyte Systems

Solid state electrolyte materials offer advantages over liquid-based alternatives in Li-ion battery application, especially in terms of safety, durability, and overall performance:

Safety Enhancement Mechanisms

- Total removal of flammable organic solvent components present in traditional electrolytes, which significantly lowers the risk of combustion, thermal runaway, and explosive failure modes.
- Preventing electrolyte containment failures, which are frequently seen in liquid systems, reducing the risk of operational failure and environmental contamination [7].

Durability and Performance Longevity

- Development of stable electrode-electrolyte interfaces resistant to degradation processes typically observed with liquid electrolytes

- Significant reduction in parasitic reactions including electrolyte decomposition pathways, preserving performance characteristics over extended operational periods [7]

Structural Integrity Preservation

- Effective suppression of lithium dendrite formation crystalline structures that propagate through liquid electrolytes causing internal short circuit events substantially reducing catastrophic failure probabilities

Energy Storage Capacity Advancement

- Compatibility with lithium metal anode materials, enabling substantially higher energy density configurations compared to graphite-based anodes typically employed in liquid electrolyte systems.

Environmental Adaptability

- Maintenance of consistent performance parameters across extreme temperature conditions, unlike liquid electrolytes which demonstrate significant operational limitations in high-temperature or sub-zero environments [7].

Design Versatility

- Facilitation of reduced-profile, space efficient, and conformable battery configurations, creating new application opportunities in wearable electronic devices, implantable medical technologies, and advanced energy storage systems.

1.6 Categorization of Solid Electrolyte Systems

Solid electrolytes come in three main types based on what they are made of and how they transport charged particles: ceramic, polymer, and composite materials.

1.6.1 Ceramic Solid Electrolytes

Scientists have spent a lot of time studying ceramic solid electrolytes because they conduct ions very well and can handle high temperatures without breaking down. This group includes materials like garnet-type lithium lanthanum zirconium oxide ($Li_7La_3Zr_2O_{12}$), NASICON-type structures, and perovskite-based electrolytes. These materials create good

pathways for lithium ions to move through them. Among these, garnet-type LLZO shows great potential because it works well with lithium metal and resists the formation of dangerous needle-like structures called dendrites. However, ceramic electrolytes tend to be hard and brittle like pottery, making them difficult to use in batteries that need to bend or flex [8].

1.6.2 Polymer Solid Electrolytes

Polymer solid electrolytes are more flexible and easier to work with than ceramics. Common examples include materials based on polyethylene oxide (PEO), which allow lithium ions to move through while still being able to bend and flex.

The main drawback of polymer electrolytes is that they do not conduct ions as well as ceramics do at room temperature. Researchers try to improve this by adding salts or mixing in tiny inorganic particles to enhance their performance[9] .

1.6.3 Composite Solid Electrolytes

Composite solid electrolytes take the best features from both ceramics and polymers. They basically mix ceramic particles into a polymer base, creating a material that balances good ion conductivity, flexibility, and stability. This helps to solve the problems like - it reduces the brittleness of ceramics while improving the conductivity issues of polymers[9], [10].The development of this solid electrolyte is crucial for making better lithium ion batteries with improved safety, longer life, and better performance. Ongoing research in this field continues to drive advancements in future energy storage solution.

1.7 Understanding LLZO Garnet Frameworks for Solid-State Battery Applications

Atomic Organization in LLZO Structures

There are two main crystalline forms of LLZO: tetragonal and cubic. The atomic architecture of LLZO garnet frameworks exhibits a precise distribution of elements across particular crystallographic positions. Although the crystal structure of LLZO is the same in both phases, the distribution of lithium atoms varies. During the tetragonal phase,

- The Li^{+} ions predominantly occupy tetrahedral (24d) and octahedral (96h) positions, creating an interconnected network that serves as pathways for ion transport. This distribution is fundamental to the materials ionic conductivity performance.
- La^{3+} cations are situated in dodecahedral (16a) sites, providing essential structural integrity to the overall garnet framework.
- Zr^{4+} ions are positioned within octahedral (16c) sites, contributing significantly to the overall structural rigidity of the crystal lattice[11].

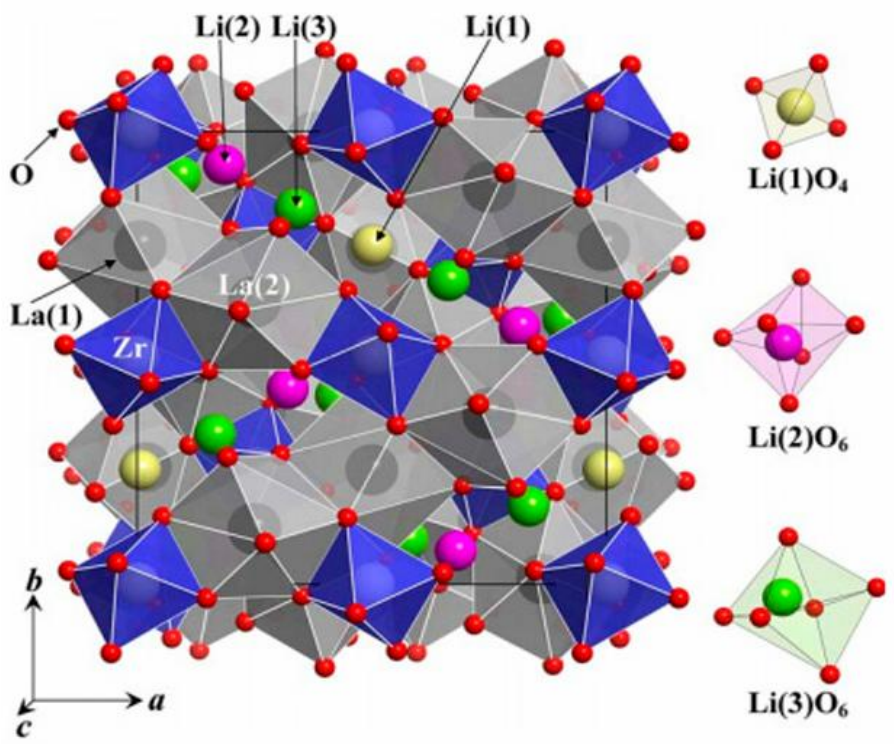

Figure 4: Crystal structure of tetragonal LLZO[12]

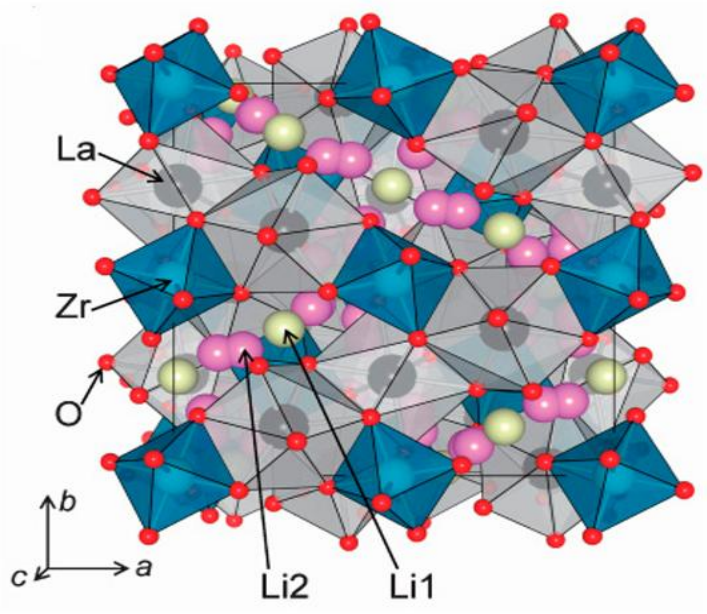

Figure 5: Crystal structure of cubic LLZO[12]

- Cubic LLZO: Exhibits higher symmetry where all axes are equal (a = b = c) and angles remain 90°. This phase is typically found at elevated temperatures.
- Tetragonal LLZO: Displays slightly lower symmetry, with two axes being equal but distinct from the third ($a = b \neq c$) while still retaining at 90° angles. This form emerges due to structural distortions, often induced by temperature variations.

Materials demonstrating superior ionic conductivity typically feature crystal structures with unobstructed migration channels for ion transport. In LLZO garnet structures, the cubic polymorph provides an advantageous three-dimensional conduction network that facilitates efficient lithium ion movement. In contrast, more restrictive arrangements, such as the tetragonal configuration, tend to constrain ionic mobility, resulting in diminished conductivity performance.

Understanding the Transformation of LLZO Crystal Phases

As known LLZO exists in two primary crystalline forms: tetragonal and cubic. The shift from the tetragonal phase to the cubic phase significantly affects its ionic conductivity, making it an important aspect in solid-state lithium ion battery research.

Phase Transition Observations

Using X-ray diffraction (XRD) analysis, Adams and Rao observed a gradual transformation of tetragonal LLZO into cubic LLZO. Initially, at lower temperatures, the tetragonal structure is identifiable by two Bragg peaks (211 and 112). However, as the temperature increases, the 211 peak strengthens, while the 112 peak gradually disappears, completely vanishing beyond 450 K. This disappearance signifies the clear transition of LLZO into its cubic phase[13].

Factors Affecting the Phase Transition

The transition from tetragonal to cubic LLZO is influenced by dopants and processing methods. To optimize battery performance, researchers are looking into ways to stabilize the cubic phase.

Additionally, the distribution of lithium atoms varies in the two phases, but the LLZO crystal structure stays the same:

- Higher conductivity is made possible by the additional empty sites that cubic LLZO offers for Li-ion movement.
- Ion mobility and conductivity are restricted by the fully occupied positions of tetragonal LLZO.

Furthermore, while the tetragonal phase experiences a phase transition at roughly 100–150°C in air, cubic LLZO is typically stable in air. For many real-world applications where stability under operating conditions is crucial, cubic LLZO is a more desirable material due to its thermal sensitivity[14].

For solid-state battery technologies to advance, it is essential to comprehend and regulate the phase transition between tetragonal and cubic LLZO. Researchers seek to improve ionic stability by refining dopants, synthesis methods, and processing conditions.

CHAPTER 2
LITERATURE REVIEW

Extending earlier research, our work focuses on the garnet-type solid electrolyte $Li_7La_3Zr_2O_{12}$ (LLZO) with the specific goal of improving its structural properties and ionic conductivity for advanced battery applications.

2.1 Need of doping in LLZO

By strategically doping $Li_7La_3Zr_2O_{12}$ (LLZO) with elements like Sr, Ta, Nb, or Ga, critical lithium vacancies are introduced, greatly enhancing ionic mobility pathways. In addition to improving conductivity, this substitutional method stabilizes the cubic crystal structure, which is necessary for optimum performance. These structural changes also enhance interfacial stability with lithium metal electrodes, improve synthesis methods, and drastically decrease dendritic formation. Doped LLZO is now a very promising electrolyte for advanced solid state energy storage applications thanks to these developments [15].

Substitutional incorporation and interstitial integration are the two main methods for adding dopants to $Li_7La_3Zr_2O_{12}$, and each has a unique impact on the material's performance properties.

The substitutional approach involves purposefully substituting foreign elements for particular lattice sites within the LLZO crystalline framework. Notably, positions typically occupied by La^{3+} or Zr^{4+} cations are regularly filled by dopants like Sr^{2+}, Ta^{5+}, Nb^{5+}, and Ga^{3+}. This deliberate substitution improves lithium mobility while also facilitating the preservation of the cubic phase. In order to create optimized conduction channels, the mechanism entails calculating deficiencies in the lithium sublattice.

Instead of replacing existing atomic positions, the interstitial integration method places dopant species inside the LLZO crystal structure's vacant void spaces. By creating additional pathways that enable more effective lithium ion migration throughout the material, this alternative doping technique can further improve ionic conductivity.

2.2 Garnet Type Li-Ion Conductor (LLZO)

The study uses a modified polymer complex process to present a low temperature synthesis method for garnet type LLZO. With the use of citric acid and ethylene glycol as processing aids, crystallization to tetragonal and cubic configurations was accomplished at 700°C and 1100°C, respectively. The use of high-energy mechanical milling reduced particle dimensions and promoted crystal formation. The material's potential use in fully solid lithium-ion energy storage systems was validated by its ionic conductivity values of 6.4×10^{-7} Scm^{-1} (tetragonal) and 1.4×10^{-4} Scm^{-1} (cubic)[16].

A liquid-phase sol-gel preparation method for cubic LLZO, a high-performance ion-conducting solid electrolyte, was investigated by the researchers. At 600°C, the cubic LLZO structure formed, producing nanometric intergranular regions with mean crystallite dimensions of 260 nm, which are roughly 13 times more refined than the results of traditional solid-state fabrication. The compound showed unique transport properties due to its nanoscale architecture, demonstrating its suitability for next-generation lithium-ion power cells with an ionic conductivity of 0.4 mS cm^{-1} at room temperature (298 K)[17].

The introduction of LLZO (M = Nb, Ta) oxide compounds by Thangadurai and associates in 2003 marked a significant breakthrough in lithium ion conducting materials. By identifying these materials as remarkable garnet-structured lithium ion conductors, this important discovery laid the foundation for future advancements and scientific research in this specialized area[18].

Garnet-type LLZO nano powders were fabricated using an adapted sol-gel Pechini synthesis approach. The cubic structural arrangement developed at 978 K, while transformation to tetragonal configuration occurred beyond 997 K. The results from conventional solid-state preparation techniques were consistent with the tetragonal variant lithium ion conductivity, which measured 3.12×10^{-7} S/cm at room temperature (298 K) with activation requirements of 0.67 eV[19].

The pulsed laser deposition was used to create thin films on both $SrTiO_3$ and Sapphire substrates. The films were amorphous at first and had a lithium-ion conductivity of 3.35×10^{-7} S/cm. after being treated with pulsed laser annealing, the conductivity rose to 7.36×10^{-7} S/cm. They also confirmed that the films remained electrochemically stable when in

contact with lithium metal, indicating that they have a great deal of potential for use in lithium ion battery technology[19], [20].

The study used pulsed laser deposition to create aluminium-doped LLZO epitaxial thin films in order to investigate the transport characteristics of lithium ions. According to their analysis, when measured at 298 K, films with (001) orientation had an ionic conductivity of 2.5×10^{-6} S/cm, whereas those with (111) orientation had a superior conductivity of 1.0×10^{-5} S/cm. According to their findings, the three-dimensional migration pathways were impacted by the addition of Al^{2+} ions, which reduced the quantity of mobile lithium ions. Furthermore, lattice mismatch effects were blamed for variations in conductivity[21].

Garnet-type $Li_{7-x}La_3Zr_2O_{12-1/2x}$ materials with both cubic and tetragonal crystal structures were synthesized using a sol-gel technique. Grain boundary conductivity of 1.39×10^{-4} S/cm and bulk conductivity of 5.69×10^{-4} S/cm for the cubic phase at room temperature (25°C) was reported. Through immersion tests in saturated LiCl solution at 50°C for seven days, the stability of the cubic phase was verified; no discernible alterations in material structure or conductivity were noted during this time. These materials are further established as promising candidates for applications in next-generation lithium-ion batteries due to their exceptional stability[22].

Amorphous Li-La-Zr-O thin films were studied and lowering activation energy barriers and increasing ionic conductivity (4×10^{-7} S/cm) at the deposition power to 40 W were reported. These amorphous materials are positioned as strong candidates for incorporation into all-solid-state thin-film lithium ion batteries as a result of this work. It has been reported that the amorphous structure improved the materials stability and functional performance by fostering a more uniform and dense surface morphology[23].

In another significant contribution, high-purity cubic-phase $Li_7La_3Zr_2O_{12}$ powders were successfully synthesized employing a solution-based methodology. This material demonstrated lithium ion conductivity measuring approximately 1.67×10^{-4} S/cm. When incorporated into a prototype all-solid-state battery configuration, the electrolyte enabled a specific discharge capacity of 3.4 m Ah/g reportedly the highest performance achieved with this particular electrolyte material to date[24].

2.3 Single Doping

Gallium-doped garnet electrolytes were studied as potential components for solid-state lithium ion batteries. The research revealed an impressive peak lithium-ion conductivity of 1.46 mS/cm at room temperature when the gallium doping concentration reached 0.25 a.p.f.u. The investigation uncovered fundamental mechanisms connecting lithium-ion mobility and phase transitions that contribute significantly to the enhanced conductivity performance[25].

Some report observed the important tetragonal-to-cubic phase transition in garnet-type ceramic electrolytes by introduction super-valent cation substitution at the 24c site. The findings demonstrated that cerium (Ce^{4+}) doping effectively stabilized the cubic phase when Ce concentration was 0.2 a.p.f.u. or higher. This stabilization effect was attributed to the creation of lithium vacancies while maintaining oxygen stoichiometry throughout the structure. Despite this phase stabilization, the ionic conductivity of the Ce-doped samples proved lower than their aluminium and tantalum-doped counterparts, primarily due to cerium dioxide (CeO_2) precipitation occurring at grain boundaries [26].

It was seen that iron-stabilized LLZO electrolytes. While these materials demonstrated high ionic conductivity measuring 1.1 mS cm^{-1}, unfortunately it showed poor stability when in contact with lithium metal. This interfacial degradation resulted in the formation of a thick tetragonal LLZO interlayer, which caused high impedance (approximately 1 kΩ cm^2) and ultimately limited the material practical application in all-solid-state battery systems[27].

The study explored a promising garnet-related oxide synthesized through solid-state reaction methods. Their findings revealed a cubic structure with impressive lithium ion conductivity, measuring 2.5×10^{-4} S/cm at room temperature (25°C). With an activation energy of just 0.42 eV, this material shows considerable potential as a solid electrolyte for next-generation lithium ion battery applications[3].

Lithium garnet-type oxides with the composition $Li_{7-x}La_3Zr_{2-x}Nb_xO_{12}$, where x ranged from 0 a.p.f.u. to 2 a.pf.u. were investigated. The solid-state reaction synthesis approach revealed an interesting correlation: increasing niobium content enhanced lithium ion conductivity, which peaked at approximately 0.8 mS/cm at room temperature. The activation energy reached its lowest point of about 30 kJ/mol when x equalled 0.25 a.p.f.u.

Notably, these materials demonstrated exceptional electrochemical stability with no observable reactions occurring up to 9 volts versus Li^+/Li[28].

The $Li_{7-x}La_3Zr_{2-x}Ta_xO_{12}$ garnets (x = 0-2) was synthesized using solid-state synthesis. The findings showed that single cubic phase was formed at x = 0.2 to 2, with peak conductivities of 9.6×10^{-4} S/cm (bulk) and 6.9×10^{-4} S/cm (total) at room temperature for x = 0.3 a.p.f.u. and x = 0.2 a.p.f.u. respectively[29].

The study was done with W-doped LLZO ceramics (x = 0-0.55) and found that tungsten doping stabilizes the cubic phase and improves density to 96%. The materials achieved 6.6×10^{-4} S/cm conductivity at 25°C with excellent lithium stability, maintaining 94% capacity after 20 cycles[30].

C. Deviannapoorani [31]synthesized lithium garnets with pyrochlore via solid-state reactions. Tetragonal phase formed at 950°C while cubic phases appeared at 1200°C. Al-doping directly stabilized the cubic phase at 950°C, achieving 4.43×10^{-4} S/cm conductivity at 30°C with 93% relative density.

Ge-doped garnet-type LLZO was investigated as a potential solid electrolyte for lithium ion batteries. Doping with Ge at the lithium sites increases the number of lithium ion vacancies, thereby improving ionic conductivity. XRD analysis confirmed the formation of a stable cubic phase, while SEM studies revealed details of surface morphology and elemental composition. The material achieved a peak ionic conductivity of 7.23×10^{-4} S/cm at room temperature, with a low activation energy of 0.56 eV. These results indicate that Ge-doped LLZO holds strong potential for future energy storage technologies[32].

2.4 Co-Doping

Daniel Rettenwander and colleagues [33] investigated the effects of aluminium and gallium co-substitution in LLZO materials. The research revealed that the ratio of Al substitution significantly influences the structural phase of the material. This co-substitution approach successfully lowered activation energy to 0.26 eV while enhancing ionic conductivity from 2.6×10^{-4} to an impressive 1.2×10^{-3} S/cm. It is also found that increasing gallium content improved several key properties including densification, grain size, and reduced the area-specific resistance to just 24 Ω cm^2.

Sumaletha Narayanan et al.[34] studied Y and Nb co-doped garnet-type materials synthesized through traditional solid-state reaction methods. The findings highlighted that $Li_{6.5}La_3Nb_{1.25}Y_{0.75}O_{12}$ demonstrated exceptional ionic conductivity measuring 2.7×10^{-4} S/cm at room temperature while maintaining excellent structural and chemical stability up to temperatures between 400–600°C. The study demonstrated that Y^{3+} doping was effective in boosting ionic conductivity, surpassing the performance of other dopant materials.

L. Dhivya and Ramaswamy Murugan [35] examined how simultaneous substitution of Y^{3+} for La^{3+} and Ta^{5+} for Zr^{4+} affected garnet-type LLZO materials. The study demonstrated that optimal doping effectively enhances stabilization of the high-conductivity cubic phase while reducing grain boundary resistance and improving bulk resistance. Among the various compositions tested, the materials achieved maximum lithium ion conductivity of 4.36×10^{-4} S/cm when processed at 1200°C.

R. Murugan, V. Thangadurai, and W. Weppner [36] investigated garnet-based solid electrolytes with particular attention to lithium content. The research highlighted that lithium concentration significantly influences ionic conductivity properties, with the highest total and bulk conductivities of 1.5×10^{-4} and 1.8×10^{-4} S/cm at 50°C achieved when x=1.0 a.p.f.u.. The findings confirmed that increased lithium concentration effectively reduced grain boundary resistance and enhanced overall conductivity performance.

S. Narayanan, V. Epp, M. Wilkening, and V. Thangadurai [34]investigated $Li_{6.5}La_{2.5}Ba_{0.5}ZrTaO_{12}$, a cubic garnet-type electrolyte, highlighting its excellent lithium-ion transport and structural stability up to 673 K. Bulk conductivity values align with prior research, confirming its potential for solid-state lithium ion batteries. Long-range ion transport properties were investigated using NMR and impedance spectroscopy. Additionally, it demonstrates chemical compatibility with high-voltage cathode materials like $Li_2FeMn_3O_8$, ensuring stability at elevated temperatures.

Wolfgang G. Zeier and colleagues [37] analysed how the ionic radius of M^{2+} affects $Li_6MLa_2Ta_2O_{12}$ garnets. The detailed investigation revealed that larger ionic radii increase unit-cell parameters, effectively broadening lithium conduction pathways and enhancing

ionic conductivity by lowering activation energies, ultimately improving lithium ion transport throughout the material structure.

Mukta Aote et al. [38]explored the effects of co-doping on LLZO solid electrolytes with gallium (Ga) and germanium (Ge). The research showed that Ga doping improves lithium ion conductivity by generating lithium vacancies, while Ge serves as an effective sintering aid, helping to stabilize the cubic phase at lower synthesis temperatures. Among the compositions studied, the sample with 0.20 a.p.u.f. of Ga demonstrated the highest ionic conductivity, reaching 5.09×10^{-4} S/cm, and exhibited a low activation energy of 0.25 eV. These results highlighted the potential of this composition for application in all-solid-state lithium ion batteries (ASSLIBs) and are consistent with prior studies emphasizing the role of co-doping in enhancing LLZO performance.

Muktai Aote and A. V. Deshpande study [39] concentrated on co-doping garnet-type LLZO with Ge and Ta to increases Li-ion conductivity for use in All- Solid -State Batteries(ASSBs). At room temperature, the ceramic sample with 0.25 a.p.f.u. of Ta and a low activation energy of 0.25 ev showed the highest ionic conductivity of 6.61×10^{-4} S/cm after being sintered for 7.3 hours at 1050°C. SEM and density analysis provided information about the microstructure, while X-ray diffraction verified the development of a stable cubic phase. Over a five month period, the material also showed outstanding air stability, indicating its potential as a dependable solid electrolyte for ASSBs.

Conductivity enhancement in garnet-structured LLZO was achieved by Kumazaki's team[19] through Silicon (Si) and Aluminium (Al) incorporation. This modification effectively reduced resistance at grain boundaries, yielding ionic conductivity values of 6.8×10^{-4} S/cm at room temperature (298 K). The presence of non-crystalline Li-Al-Si-O phases and nanocrystalline $LiAlSiO_4$ at grain interfaces promoted efficient ion migration, establishing LLZO as a compelling candidate for solid-state energy storage applications.

2.5 Multi Doping

LLZO-based garnet structures represent essential solid electrolytes for future solid-state battery development, offering notable ionic conductivity and structural reliability. Incorporating dopants such as Al, Ga, Rb, Nb, and Ta at lithium, lanthanum, and zirconium

positions substantially enhances ion movement and material characteristics. Utilizing sol-gel preparation techniques allows exact compositional management, creating consistent grain morphology and superior functional properties. The implementation of three simultaneous dopants has produced LLZO materials featuring pristine cubic crystallinity, few unwanted phases, and remarkable conductivity values. This study validates the potential of modified LLZO as a highly effective electrolyte for next generation energy storage systems[40].

The Al-substituted composition $Li_{6.15}La_3Zr_{1.75}Ta_{0.25}Al_{0.2}O_{12}$ exhibited ionic conductivity of 0.37 mS/cm when tested at room temperature (298 K), with an energy barrier of 0.30 eV. Its gallium-containing $Li_{6.15}La_3Zr_{1.75}Ta_{0.25}Ga_{0.2}O_{12}$ performed marginally better, showing enhanced conductivity (0.41 mS/cm at 298 K) and requiring less activation energy (0.27 eV)[37].

Two compounds with mixed alkaline earth metals, $Li_6Ba_{0.5}Sr_{0.5}La_2Ta_2O_{12}$ and $Li_6Sr_{0.5}Ca_{0.5}La_2Ta_2O_{12}$, were synthesized using conventional solid-state reaction methods. The barium-strontium variant demonstrated conductivity measuring of 7.1×10^{-3} S/cm with an activation energy of 0.45 eV. The strontium-calcium version showed lower performance with conductivity reaching 3.2×10^{-3} S/cm and requiring slightly more activation energy of 0.50 eV [41].

The multi-element doped garnet structure $Li_{6.65}Ga_{0.05}La_{2.95}Ba_{0.05}Zr_{1.75}Ta_{0.25}O_{12}$ achieved superior results with ionic conductivity reaching 0.72 mS/cm at standard room temperature, which further improved to 1.24 mS/cm when heated to 60 °C[42].

Objective of Present Work

Our previous discussion evaluated battery technologies, focusing on the rationale behind Li-ion battery dominance in the market, the emerging significance of solid-state electrolytes, and a detailed examination of the garnet-structured LLZO electrolyte and its distinctive characteristics. It was noted that Niobium can be substituted at the site of Zirconium which leads to increased number of vacancies for lithium ion to migrate. Moreover, along with Nb, Ga can stabilize the cubic structure and can lead to remarkably high conductivity of the orders of 10^{-3} S/cm at room temperature, acts as sintering aid, and

Sr doping can give access to fine tuning in cubic structure and increase of Li^+ concentration, which helps to optimize bulk conductivity. In the forthcoming section, the experimental methodologies employed for material preparation and analytical techniques will be outline before presenting and interpreting the research outcomes from present investigation.

The following work has been carried out:

1. Synthesis of pure LLZO solid electrolyte and Ga, Sr and Nb doped $Li_{6.45-x}Ga_{0.20}La_{2.95}Sr_{0.05}Zr_{2-x}Nb_xO_{12}$ series of compounds with varying compositions (x = 0.0,0.05,0.10, 0.15).
2. XRD of pure LLZO and tri-doped $Li_7La_3Zr_2O_{12}$
3. Density measurements for each compositional variant.
4. Investigation of microstructural features and morphology through SEM imaging.
5. Measurement of electrical conductivity of all the samples of the series.
6. Determination of ionic transport number to evaluate charge carrier contribution in all prepared samples.

CHAPTER 3
SYNTHESIS AND CHARACTERIZATION

3.1 Material preparation

The meticulous preparation of samples is essential when synthesizing advanced materials for diverse applications. The following procedures detail the systematic approach adopted for the preparation of the base material as well as the dopant samples. The synthesis of both pure LLZO and its Ga, Sr and Nb doped variant was carried out using the solid-state reaction method.

This process enhances mechanical strength by promoting diffusion-driven bonding between particles, reduces porosity, increases particle contact area, and encourages grain growth and densification, which are essential for achieving high ionic conductivity in solid electrolytes.

3.1.1 Preparation of Pure $Li_7La_3Zr_2O_{12}$ (LLZO)

Lithium carbonate (Li_2CO_3), Lanthanum oxide (La_2O_3), and Zirconium dioxide (ZrO_2) were meticulously chosen and accurately measured based on their stoichiometric proportions. To compensate for lithium evaporation during thermal processing, an additional 10% of Li_2CO_3 was incorporated. Lithium tends to volatilize at elevated temperatures, leading to a reduction in the lithium content in the final material. Adding additional Li_2CO_3 helps maintain the proper stoichiometric balance, ensuring the synthesized material achieves optimal composition and performance.

Dry Mixing: Using a mortar and pestle, the precisely measured ingredients were thoroughly mixed for 90 minutes. This process is also referred to as dry mixing. All of the components were distributed uniformly.

Wet Mixing: Wet mixing was used to increase compositional homogeneity. Acetone was added to the mixture, which improved mixing efficiency and helped with efficient grinding.

Calcination: Using a muffle furnace, the finely ground powder was heated to 900°C for eight hours in an alumina crucible. In order to ensure material stability and functionality, this step was crucial for removing impurities and promoting phase transformation.

Re-grinding and Pellet Formation: An extra hour was spent grinding the calcined powder. In order to ensuring consistency and structural integrity, pellets were subsequently formed using a hydraulic pressing technique at a pressure of four tons.

Sintering – The formed pellets were sintered at 1050°C for 8 hours within the mother powder. During this stage, an alumina lid was placed over the crucible during the sintering process to minimize lithium loss and maintain the correct stoichiometry. This procedure promoted densification of the material, improving its overall properties in this step cubic phase LLZO is formed.

3.1.2 Preparation of Ga, Sr and Nb doped LLZO

1.Formulation - The samples of the $Li_{6.45-x}Ga_{0.20}La_{2.95}Sr_{0.05}Zr_{2-x}Nb_xO_{12}$ series were prepared with varying Nb concentration (x = 0.0 to 0.15 a.p.f.u.) and keeping Ga content constant at 0.20 a.p.f.u. because it provides more ion channel and consequently benefits the Li-ion transportation, and Sr content constant at 0.05 a.p.f.u. because doping of Sr at La site can give access to fine tuning in cubic structure and increase of Li^+ concentration, which helps to optimize conductivity. 10% extra Li_2CO_3 was added to prevent Li loss during heat treatment.

2. Selection and Weighing - Lithium carbonate (Li_2CO_3), Lanthanum oxide (La_2O_3), Zirconium dioxide (ZrO_2), Gallium oxide (Ga_2O_3), Strontium carbonate ($SrCO_3$) and Niobium oxide (Nb_2O_5) were carefully selected and precisely weighed according to stoichiometric ratio. And similar synthesis steps from dry mixing to sintering were followed as mentioned in preparation of pure LLZO.

Table 1: Chemicals used for synthesis of pure and doped $Li_7La_3Zr_2O_{12}$

Sr. No	Chemical name	Formula	Make	Purity
1	Lithium carbonate	Li_2CO_3	Merck	>99.9%
2	Lanthanum oxide	La_2O_3	Aldrich	>99.9%
3	Zirconium dioxide	ZrO_2	Merck	>99.9%
4	Gallium oxide	Ga_2O_3	Aldrich	>99.9%
5	strontium carbonate	$SrCO_3$	Aldrich	>99.9%
6	Niobium oxide	Nb_2O_5	Aldrich	>99.9%

3.2 Characterization Techniques

Understanding the properties of newly synthesized materials requires thorough characterization. By employing multiple analytical techniques, researchers can develop comprehensive insights into a materials fundamental properties. In order to analyse prepared samples, number of complementary characterization techniques were used in this study, including X-ray diffraction (XRD), alternating current (AC) conductivity measurements, density determination, scanning electron microscopy (SEM), and transport number analysis.

3.2.1 X-Ray Diffraction Methodology

An essential method for structural analysis is X-ray diffraction (XRD), which allows scientists to distinguish between different phases in a substance. The wavelengths of X-rays, which range from angstroms to nano meters, precisely match the interplanar distance between crystallographic planes. Effective diffraction patterns can form when X-rays interact with crystalline materials because of this dimensional compatibility.

Bragg's law serves as the foundation for X-ray diffraction principal, formulated as follows:

$$\mathbf{n\lambda = 2d \sin\theta} \qquad \text{--------(1)}$$

In this equation:

- n represents an integer indicating the diffraction order
- λ denotes the X-ray wavelength used in the experiment
- d corresponds to the spacing between atomic planes
- θ is the glancing angle formed between the incident X-ray beam and the atomic planes

The crystallographic orientation of grains or single crystals, accurate measurements of the distance between atomic planes, and information about the size, shape, and internal stresses of a material are all provided by XRD analysis.

In present study the phases of the prepared samples were characterized using a RIGAKU diffractometer equipped with Cu-Kα radiation (wavelength: 1.54 Å). The diffraction data was collected across a 2θ range of 10 to 70 degrees using a step size of 0.02 degrees and a scan speed of 2 degrees per minute. The diffraction patterns obtained were subsequently matched with corresponding JCPDS reference file to confirm phase identification.

3.2.2 Density Measurement Technique

Density determination provides a method for calculating a material mass based on its volume (or conversely, its volume from mass). In current study, the density of LLZO samples were measured using Archimedes' principle, with toluene serving as the immersion liquid.

The density measurements were performed using a K-15 Classic (K-Roy) apparatus, which consisted of several key components:

- A high-precision mono pan balance (K-Roy brand with 0.01 mg accuracy)
- Toluene as the displacement medium
- A supporting wooden stand
- A standard laboratory beaker
- A wire loop assembly for sample suspension

This setup enabled precise density determination through the measurement of sample weight in air and when immersed in toluene.

Figure 6: Experimental setup for density measurement.

For density measurements, the precise protocol was followed. To hold the sample firmly, a wire with a tiny loop was first made. The wire's initial weight in air (W_1) was noted. The combined weight in air (W_2) was measured after inserting and fastening the sample in the loop.

A specially made wooden stand that fit inside the balance without coming into contact with the pan was used in order to measure weight in toluene. On this stand a beaker of toluene was placed. After submerging the wire containing the attached sample in toluene, the measured the weight (W_3) was measured. After removing the sample, only the wire is submerged in toluene and recorded the weight (W_4).

The following formula was used in the density calculation:

$$\boldsymbol{\rho_s} = \frac{(\mathbf{W_2} - \mathbf{W_1})}{((\mathbf{W_2} - \mathbf{W_3}) - (\mathbf{W_1} - \mathbf{W_4}))} \times \boldsymbol{\rho_t} \text{ --------(2)}$$

Where:

- ρ_s = Sample density
- ρ_t = Toluene density (0.86455 g/cm³)
- $(W_2 - W_1)$ = Sample weight in air
- $((W_2 - W_3) - (W_1 - W_4))$ = Weight loss of sample in toluene

To ensure precision, multiple measurements (2 to 3 times) were conducted for each sample and computed the average density value.

3.2.3 Scanning Electron Microscopy Analysis

Scanning electron microscopy (SEM) utilizes high energy electron beams to interact with sample surfaces, resulting in the emission of secondary and backscattered electrons through atomic interactions While secondary electrons primarily provide topographical details, backscattered electrons are particularly valuable for distinguishing between multiple phases within a sample.

In present work, JSM-7600 F/JEOL scanning electron microscope was used to examine samples morphology, chemical composition, and grain orientation. This technique also allows to identify structural defects and cracks. Additionally, elemental mapping was done, assigning distinct colours to different elements to visualize their spatial distribution throughout the sample. This mapping capability helped confirm phase compositions.

For quantitative analysis, particle sizes were determined from the SEM micrographs using Image-J software processing tool[43].

3.2.4 Electrical Conductivity Measurement Principles

Electrical properties in materials stem from the movement of ions or electrons, with conductivity being influenced by temperature, frequency, and chemical composition. Lithium is light and most electropositive in nature thus it is particularly valuable for lithium ion battery development.

When measuring conductivity with direct current (DC), polarization occurs at electrolyte interfaces, creating a field that opposes the applied current and causes diminishing

readings over time. This necessitates complex extrapolation techniques to determine true conductivity values.

To overcome these limitations, alternating current (AC) conductivity measurements was done across multiple frequencies. This approach allows to accurately determine bulk conductivity while also characterizing grain boundary effects, ion transport mechanisms, and double layer formation at electrode-electrolyte interfaces.

The electrical conductivity was calculated using:

$$\boldsymbol{\sigma} = \left(\frac{\boldsymbol{t}}{\boldsymbol{RA}}\right) \boldsymbol{S/cm} \quad \text{---------(3)}$$

Where:

- t represents the sample thickness
- R is the measured resistance
- A denotes the cross-sectional area

The total conductivity comprises both ionic and electronic components**:**

$$\boldsymbol{\sigma = \sigma_i + \sigma_e} \text{ ------(4)}$$

Where σ accounts for positive and negative ions contribution, while σ_i and σ_e represents holes and electrons conductivity contribution respectively.

3.2.5 Impedance measurements

The experimental setup to measure electrical conductivity is shown below:

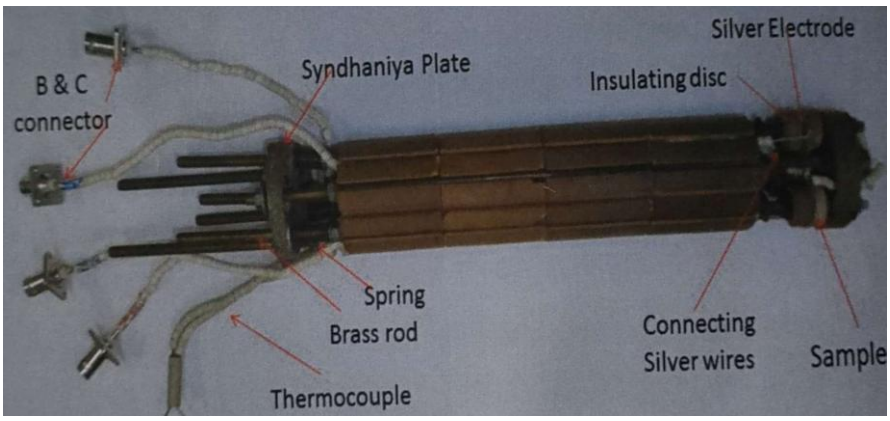

Figure 7: Sample holder for conductivity measurements

Conductivity Measurement Methodology

For electrical characterization, samples of approximately 10 mm in diameter with thicknesses between 1 to 1.5 mm were prepared. Both surfaces were coated with silver paste to create reliable electrical contacts. The prepared samples were then placed in a custom sample holder and heated in a tubular furnace with temperature regulation via a PID controller.

Impedance measurements were conducted using a high-resolution dielectric impedance analyser (Novocontrol Technologies) across a frequency range of 20 Hz to 20 MHz and temperatures from 25°C to 150°C. All measurement data was captured through computer interface for subsequent analysis.

This approach enabled comprehensive examination of both temperature and frequency-dependent electrical properties. The technique applies a small sinusoidal electrical signal to generate a linear response, allowing us to model material behaviour using equivalent circuits comprised of resistors and capacitors.

Since impedance is a complex quantity, it can be expressed as

$$|\mathbf{Z}| = \sqrt{\mathbf{Z'}^2 + \mathbf{Z''}^2} \text{-------(5)}$$

where Z' and Z'' represent the real and imaginary components. When plotting these values, a perfect resistor-capacitor parallel circuit produces a semicircle that intersects the real axis at R (low frequency) and 0 (high frequency) - known as Debye behaviour. In real materials, however, the impedance plots typically deviate from perfect semicircular forms.

From these complex impedance plots, DC conductivity values were calculated. The temperature dependence of conductivity was analysed using the Arrhenius equation:

$$\boldsymbol{\sigma = \sigma_0 \exp\left(\frac{-Ea}{kT}\right)} \text{----------(6)}$$

Where:

- σ_0 is the pre-exponential factor
- T represents absolute temperature
- E_a denotes activation energy

- k is Boltzmann's constant

3.2.6 Transport Number Analysis

For transport number measurements, sample was kept between two silver electrodes, which served as inert or irreversible electrodes. A constant 1-volt DC potential was applied across this assembly and Keithley electrometer was used to monitor current flow through the sample over time.

A characteristic decrease was observed in conductivity as polarization developed within the sample. After complete polarization occurred, the conductivity stabilized at a constant value. This steady-state conductivity represents the electronic contribution (σ_e) from the inert electrodes.

Since AC conductivity measurements are not affected by polarization effects, the AC conductivity is the total conductivity (σ_t) or zero-time conductivity. By tracking the time-dependent conductivity behaviour, the transport number was calculated using:

$$\mathbf{t_i} = \frac{(\boldsymbol{\sigma_t} - \boldsymbol{\sigma_e})}{\boldsymbol{\sigma_t}} \qquad \text{-------(7)}$$

The ionic transport number indicates the contribution of ionic conductivity to the total conductivity of the sample.

CHAPTER 4
RESULTS AND DISCUSSION

4.1 Results and Discussion of pure LLZO($Li_7La_3Zr_2O_{12}$)

4.1.1 X-Ray Diffraction Technique

The X-ray diffraction data presented in Figure 8 confirms the successful synthesis of cubic phase of pure LLZO material. Analysis revealed that the experimental diffraction pattern matches well with the standardized reference pattern documented in JCPDS file number 45-0109, which is characteristic of the cubic garnet phase of $Li_5La_3Nb_2O_{12}$. This correlation validates the successful synthesis of the cubic phase structure within the pure LLZO material. All diffraction peaks in the pattern have been appropriately labeled with their corresponding Miller indices for crystallographic identification. Although the primary conductive cubic phase was successfully synthesized, the XRD pattern exhibits shoulder peaks that indicate contamination with a secondary phase corresponding to the $La_2Zr_2O_7$ pyrochlore structure. The emergence of this unintended secondary phase can be attributed to the high-temperature conditions employed during the sintering procedure.

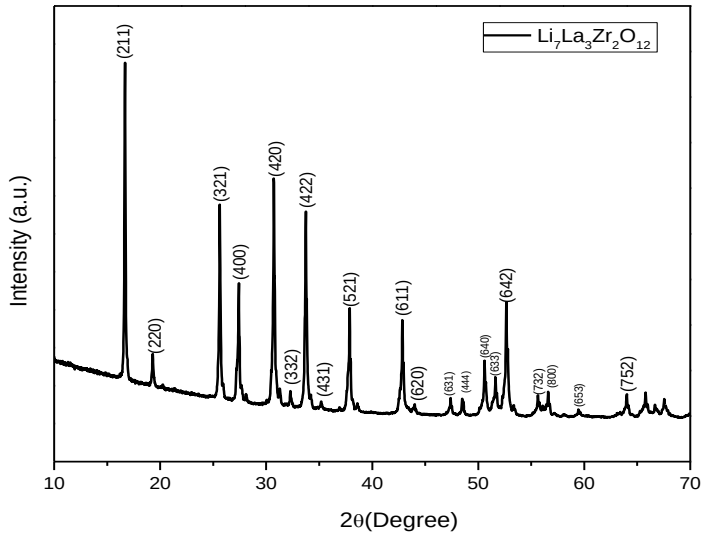

Fig 8: XRD pattern for pure LLZO

4.1.2 Density Analysis of Pure LLZO

The measured density of pure LLZO using the K-Roy instrument was approximately 4.32 g/cm³ and the corresponding relative density was 84.7%. This significant density level indicates excellent material compaction, which is essential for achieving high ionic conductivity performance and creating an effective barrier against lithium dendrite formation during battery operation.

4.1.3 Electrical Conductivity Analysis of Pure LLZO

The Nyquist plot for pure $Li_7La_3Zr_2O_{12}$, displayed in Figure 9, provides critical impedance data for conductivity determination. By examining the x-axis intercept that represents the bulk impedance of the sample, the room temperature conductivity was calculated to be 1.527×10^{-6} S/cm. The high-frequency region exhibits a slightly depressed semicircle, indicating a deviation from ideal Debye-type electrical response behaviour.

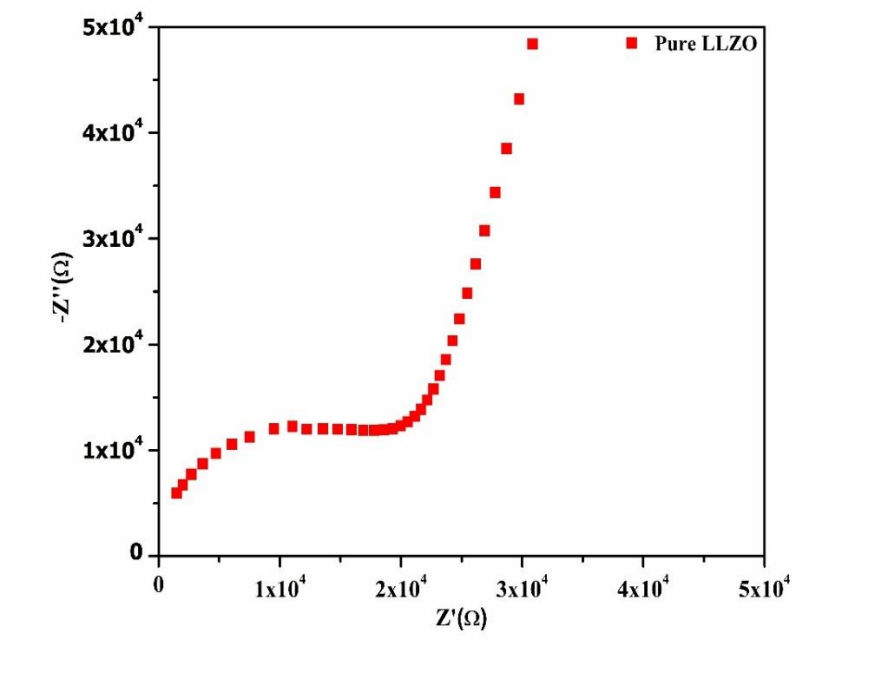

Figure 9: Nyquist plot at 25 ^{0}C of LLZO

Temperature-dependent conductivity measurements were performed using a PID controller across a temperature range spanning from 25°C to 150°C. The Arrhenius relationship between conductivity and temperature was established by plotting log(σT) v/s

1000/T as shown in Figure 10. The slope of the plot yielded an activation energy value of 0.61 eV for the ionic conduction process.

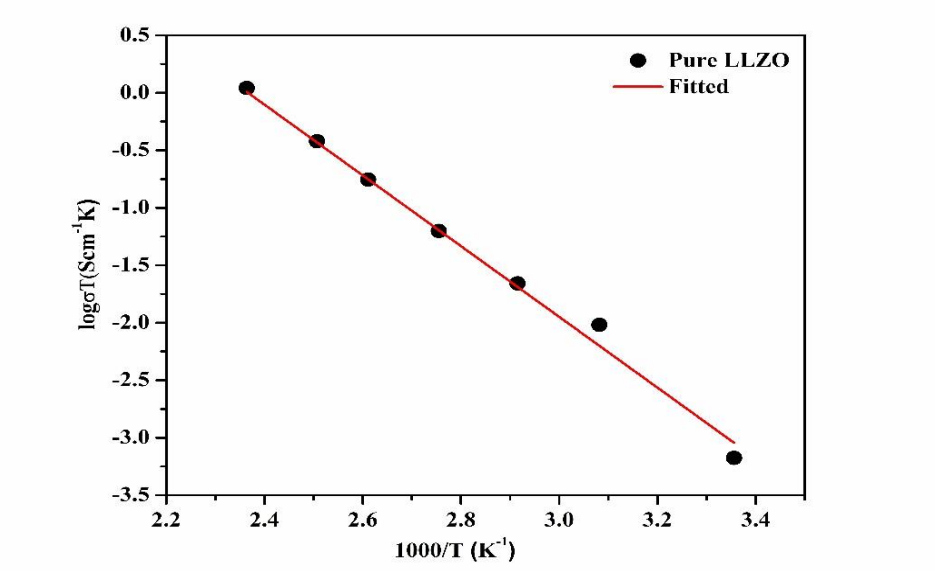

Figure 10: Arrhenius plot of pure LLZO

To further enhance the ionic conductivity of the base LLZO material, a systematic doping approach was implemented. This strategy involved substituting Niobium at Zirconium site, while simultaneously maintaining a fixed gallium (Ga_2O_3) doping level of 0.20 atoms per formula unit (a.p.f.u) at lithium site and strontium ($SrCO_3$) doping level of 0.05 a.p.f.u at lanthanum site. Comprehensive characterization of these doped compositions was conducted, with the resulting performance metrics discussed in subsequent sections.

4.2 Results and Discussion of doped LLZO

4.2.1 XRD Analysis of Ga, Sr and Nb Doped LLZO Systems

X-ray diffraction patterns for the samples of the $Li_{6.45-x}Ga_{0.20}La_{2.95}Sr_{0.05}Zr_{2-x}Nb_xO_{12}$ series (where x ranges from 0 to 0.15 a.p.f.u.) are presented in Figure 11. These samples were prepared under consistent conditions, sintered at 1050°C for 8 hours. The diffraction patterns for all samples confirm the formation of single cubic phase LLZO structures with space group Ia-3d, as verified by comparison with JCPDS file. The successful stabilization of the cubic LLZO phase through Niobium substitution is clearly demonstrated in these diffraction results. Notably, the sample containing 0.05 mole Niobium exhibits diffraction peaks of higher intensity, indicating optimal crystallization of the cubic phase at this

particular dopant concentration. Minor shoulder peaks observed in the patterns can be attributed to trace amounts of $La_2Zr_2O_7$ pyrochlore, a non-conductive secondary phase consistent with findings previously reported by Birkner and colleagues[44].

It was observed that the peaks were shifting towards higher ɵ value as Nb increases from 0 to 0.15. This shift in peak is accounted to lower ionic radius of Nb^{5+} (0.69 Å), which is smaller than that of Zr^{4+} (0.72 Å). It indicates a decrease in the lattice parameter with increase in Nb concentration.

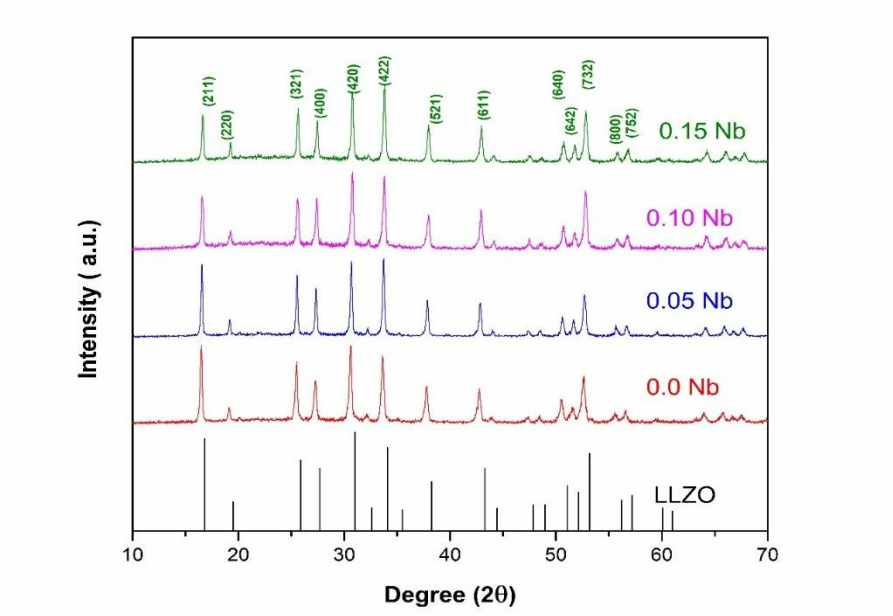

(a)

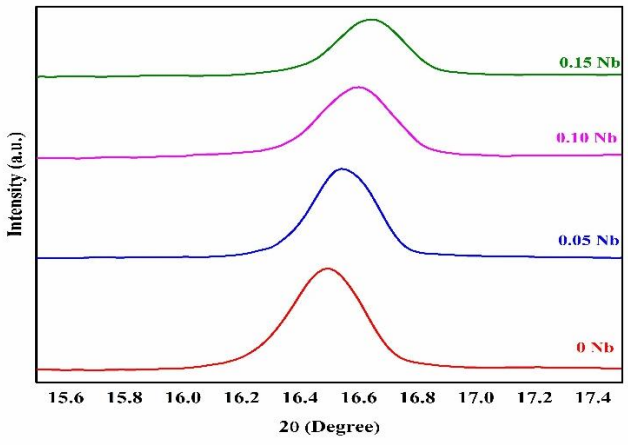

(b)

Figure 11: (a)X-Ray diffraction patterns of $Li_{6.45-x}Ga_{0.20}La_{2.95}Sr_{0.05}Zr_{2-x}Nb_xO_{12}$ (x = 0,0.05,0.1,0.15.) and (b)shifting of peaks

4.2.2 Density Analysis of Ga, Sr and Nb Doped LLZO System

Density measurements of the $Li_{6.45-x}Ga_{0.20}La_{2.95}Sr_{0.05}Zr_{2-x}Nb_xO_{12}$ series (where x ranges from 0 to 0.15) revealed a non-linear relationship between Niobium concentration and material densification. The density values exhibit an initial increase with rising Niobium content, reaching a maximum at x = 0.05 a.p.f.u. followed by a progressive decrease at higher doping levels. The sample containing x = 0.05 Nb achieved an exceptional relative density of 95.78%. The remarkable densification can be attributed to the sintering property of Nb along with the formation of $LiGaO_2$ phase resulting from the interaction between excess gallium ions and residual lithium ions. These $LiGaO_2$ formation functions as effective sintering aid, facilitating enhanced material compaction during thermal processing. These findings also align with previous research confirming the role of Ga and Sr in the LLZO at optimized concentration levels[45]. Whereas after the optimum limit of Nb, there is decrease in relative density which can be attributed to the presence of voids which can also be seen from the surface morphology images as shown in the following sections.

Table 2: Density and relative density of $Li_{6.45-x}Ga_{0.20}La_{2.95}Sr_{0.05}Zr_{2-x}Nb_xO_{12}$ (x = 0,0.05,0.1,0.15)

X	Density (g/cm^3)	Relative density (%)
0	4.57	91.41
0.05	**4.79**	**95.78**
0.1	4.59	91.80
0.15	4.46	89.20

4.2.3 Microstructural Analysis with Scanning Electron Microscopy

Scanning electron microscopy images presented in Figure 12 reveal the microstructural evolution across the $Li_{6.45-x}Ga_{0.20}La_{2.95}Sr_{0.05}Zr_{2-x}Nb_xO_{12}$ series [where x =0,0.05,0.1,0.15]. The micrograph of the 0 Nb sample (Figure 12 a) displays significant porosity throughout the microstructure. As niobium concentration increased to 0.05 an enhancement in interparticle connectivity becomes evident. Beyond the optimal niobium concentration (x

> 0.05), the microstructure begins to deteriorate. Pore size increases noticeably as niobium content exceeds its solubility threshold in the LLZO matrix. The sample with the Niobium content (x = 0.05, Figure 12 b) exhibits a significant increase in grain size, which correlates with the previously observed increase in density values. The microstructural degradation at higher doping levels confirms the existence of an optimal niobium concentration for achieving a superior material.

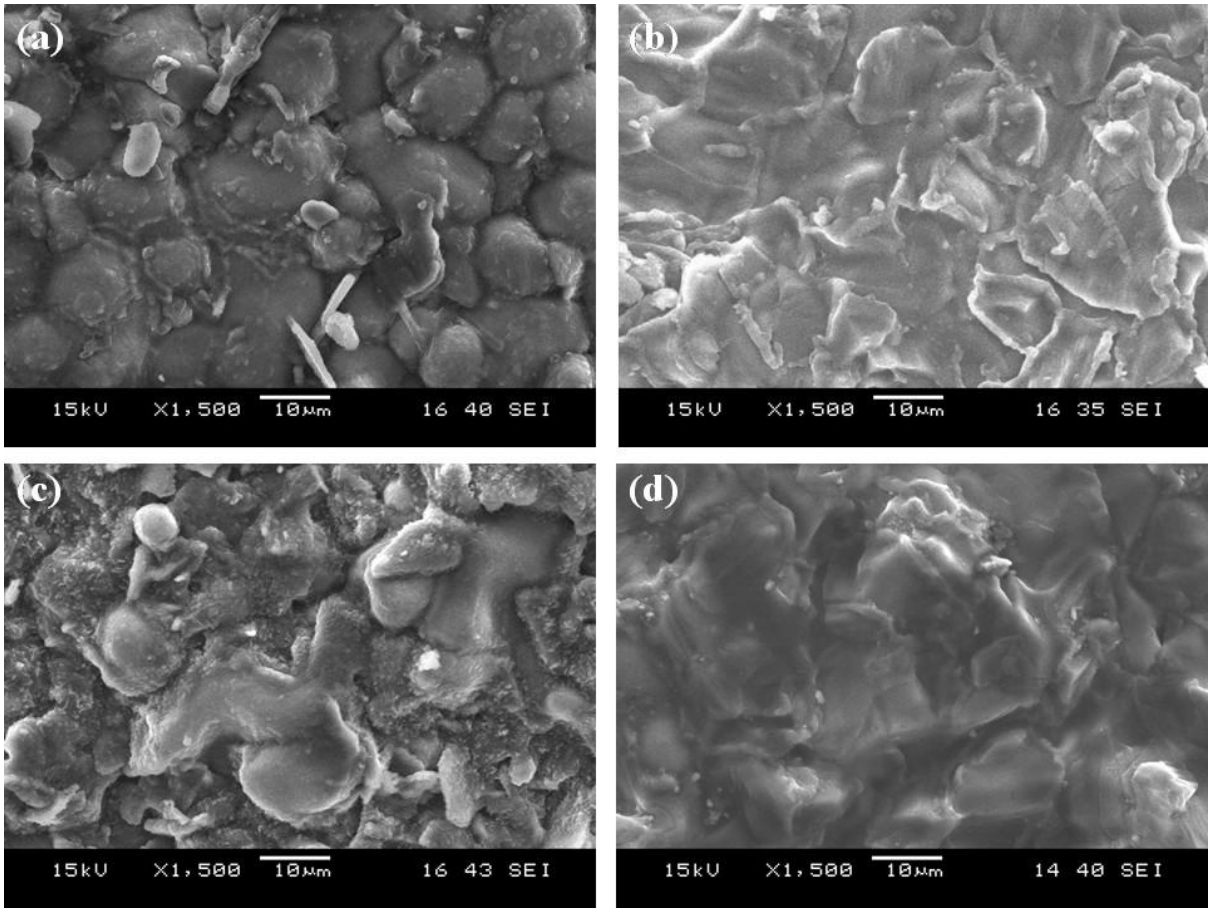

Figure 12: SEM Morphology of $Li_{6.45-x}Ga_{0.20}La_{2.95}Sr_{0.05}Zr_{2-x}Nb_xO_{12}$

(a) x=0, (b) x=0.05, (c) x=0.1, (d) x=0.15

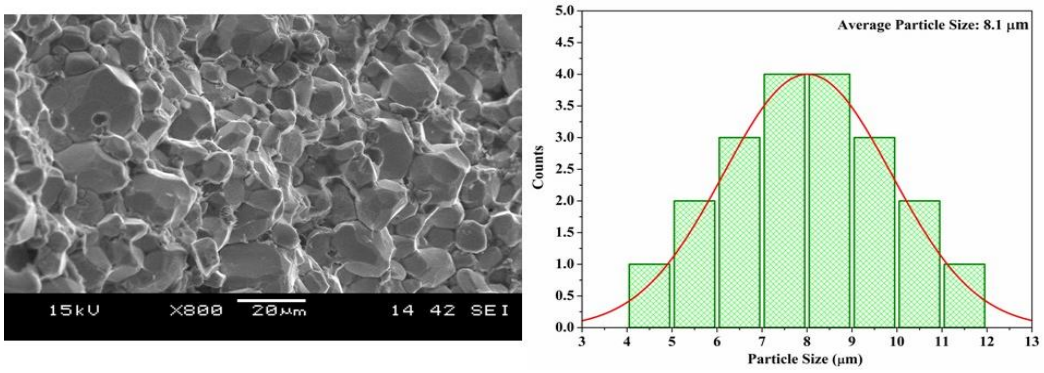

(a) (b)

Figure 13: (a) SEM of x = 0.05 and (b) average particle size distribution for x = 0.05

The average particle size was found using Cross sectional SEM of x = 0.05 and it was found to be 8.1 µm.

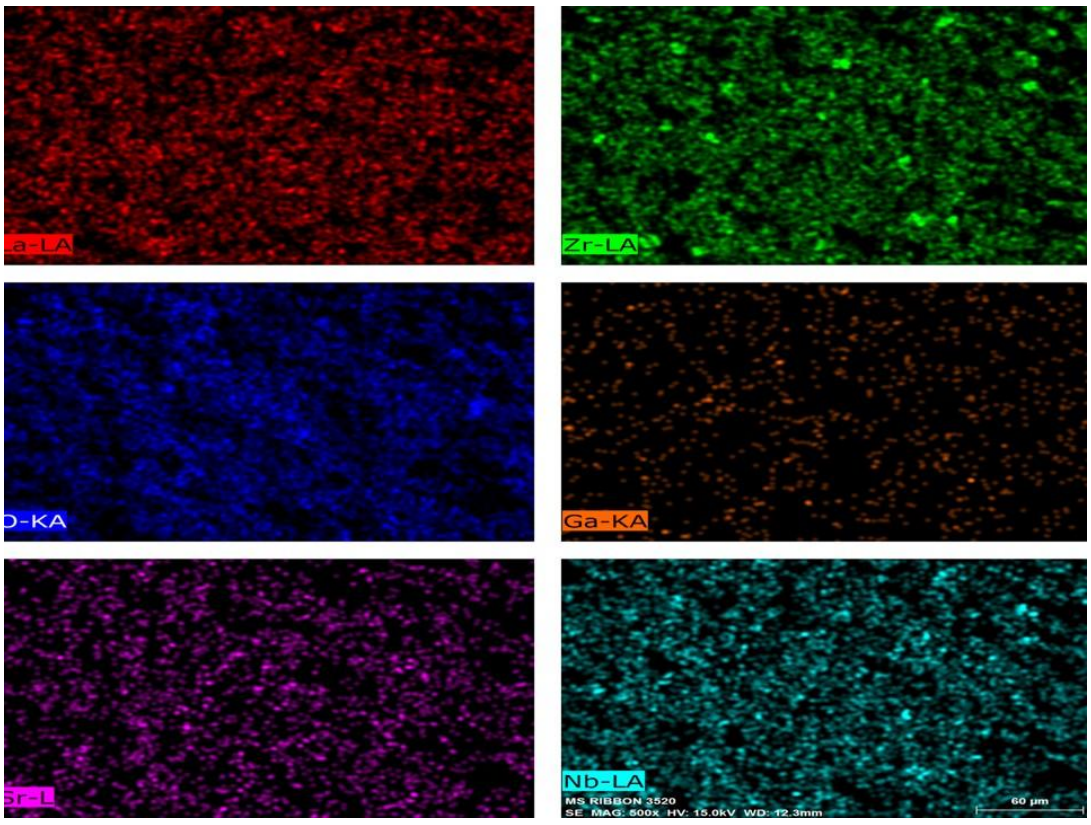

Figure 14: Elemental mapping of $Li_{6.4}Ga_{0.20}La_{2.95}Sr_{0.05}Zr_{1.95}Nb_{0.05}O_{12}$.

The elemental mapping is shown in the above figure 14 corresponding to elements of the 0.05 Nb ceramic sample. From the figure, it is observed that all the elements viz. La, Ga, Zr, Nb, Sr and O are present within the sample and are uniformly distributed all over the

ceramic. This distribution suggests that Ga, Sr and Nb are incorporated within the LLZO garnet structure. Here, Li cannot be detected due to its low energy.

4.2.4 Electrochemical Performance Analysis of Ga, Sr and Nb Doped LLZO Systems

The Nyquist plots for the series $Li_{6.45-x}Ga_{0.20}La_{2.95}Sr_{0.05}Zr_{2-x}Nb_xO_{12}$ (x = 0,0.05,0.1,0.15) are presented in Figure 15a. The bulk impedance, determined from the x-axis intercept, provides critical data for conductivity calculations. Rather than displaying clearly defined centred semicircles, these plots exhibit small semicircular arcs in the high-frequency region, indicating non-ideal Debye-type electrical behaviour.

The $Li_{6.4}Ga_{0.20}La_{2.95}Sr_{0.05}Zr_{1.95}Nb_{0.05}O_{12}$ composition (x=0.05) demonstrates superior electrochemical performance with a room temperature ionic conductivity of 2.92×10^{-4} S/cm. Analysis of the conductivity plots revealed this composition has the minimum real axis intercept among all samples, indicating lowest resistance and thus highest conductivity.

This enhanced ionic conductivity can be attributed to the synergistic effects of gallium substitution at lithium sites, strontium at lanthanum and niobium at zirconium positions, which collectively reduce the electrical resistance.

The conductivity values correlate strongly with density measurements, with the 0.05 Nb sample exhibiting both maximum density and peak conductivity. This composition achieves a conductivity two orders of magnitude higher than undoped LLZO.

Samples with niobium content exceeding x=0.05 show shifting impedance intercepts toward lower frequencies, indicating increased resistance and consequently reduced conductivity. This performance decline can be attributed to niobium solubility limitations in the LLZO structure beyond this threshold concentration along with formation of pores which leads to the obstruction in Li-ions migration.

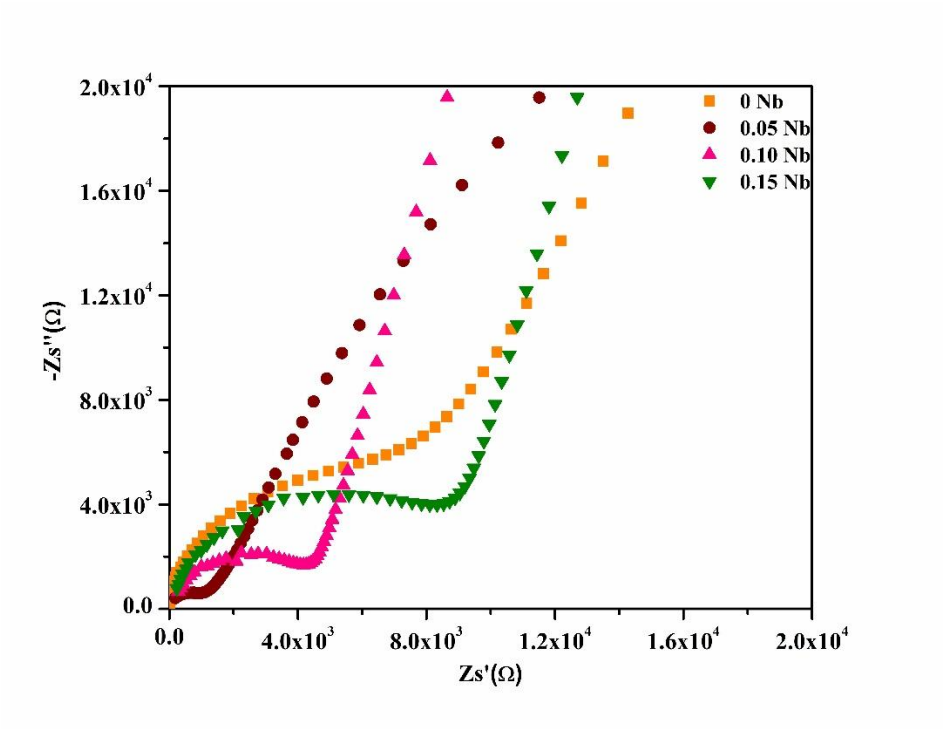

Figure 15: a) Nyquist plots at RT for $Li_{6.45-x}Ga_{0.20}La_{2.95}Sr_{0.05}Zr_{2-x}Nb_xO_{12}$ (x = 0,0.05,0.1,0.15)

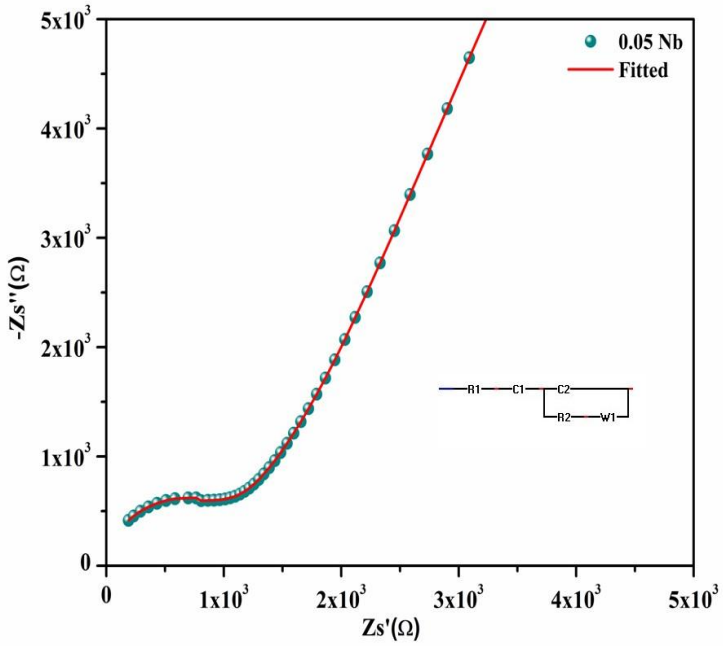

Figure 15: b) Nyquist Plot for $Li_{6.4}Ga_{0.20}La_{2.95}Sr_{0.05}Zr_{1.95}Nb_{0.05}O_{12}$ at RT with equivalent fitted circuit.

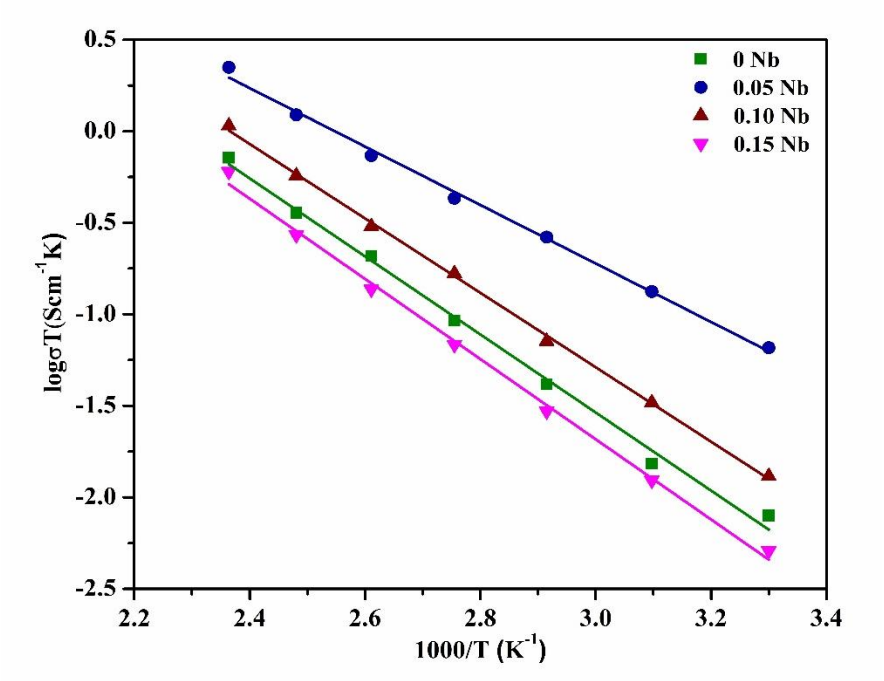

Figure 16: Conductivity as a function of temperature for

$Li_{6.45-x}Ga_{0.20}La_{2.95}Sr_{0.05}Zr_{2-x}Nb_xO_{12}$ (x = 0,0.05,0.1,0.15)

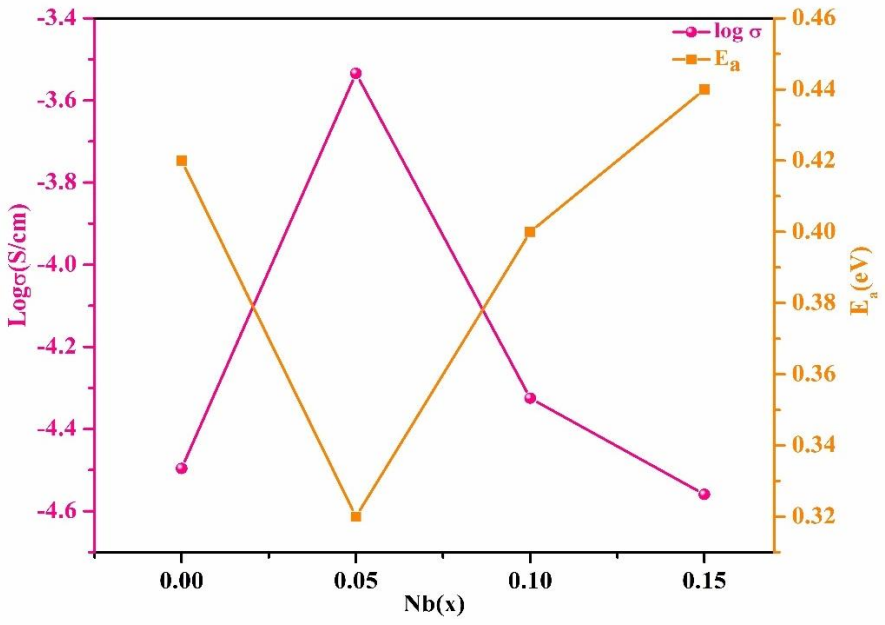

Figure 17: Variation of conductivity at 25℃ and activation energy for

$Li_{6.45-x}Ga_{0.20}La_{2.95}Sr_{0.05}Zr_{2-x}Nb_xO_{12}$ (x = 0,0.05,0.1,0.15).

Arrhenius plots for the $Li_{6.45-x}Ga_{0.20}La_{2.95}Sr_{0.05}Zr_{2-x}Nb_xO_{12}$ (x = 0 to 0.15) series are shown in Figure 16. The conductivity was measured across temperatures ranging from 25°C to 150°C. The activation energy was calculated by applying the Arrhenius equation to the slope values. The variation in ionic conductivity and activation energy as a function of Nb content is shown in Figure 17.

Table 3: Values of conductivity at RT and activation energy for

$Li_{6.45-x}Ga_{0.20}La_{2.95}Sr_{0.05}Zr_{2-x}Nb_xO_{12}$ (x = 0,0.05,0.1,0.15).

X	σ at RT	E_a (eV)
0	3.19×10^{-5}	0.42
0.05	$\mathbf{2.92 \times 10^{-4}}$	**0.32**
0.10	4.73×10^{-5}	0.40
0.15	2.76×10^{-5}	0.44

The findings demonstrate an inverse relationship between activation energy and conductivity. Specifically, when x = 0.05, the material exhibits both the lowest activation energy and the highest ionic conductivity, reaching 2.92×10^{-4} S/cm. This composition represents the optimal Niobium concentration for enhanced ionic transport in this garnet-type solid electrolyte system. These results suggest that strategic niobium doping in the garnet structure creates an optimal balance of charge carriers and mobility pathways, which is crucial for developing high performance solid-state electrolytes for advanced battery applications.

4.2.5 DC Conductivity Measurement

The ionic transport characteristics of the optimized $Li_{6.45-x}Ga_{0.20}La_{2.95}Sr_{0.05}Zr_{2-x}Nb_xO_{12}$ (x = 0.05) composition were evaluated using DC polarization methodology. Figure 18 presents the DC conductivity measurements recorded over an extended 300-minute period, with data acquisition performed via a Keithley electrometer.

To quantify the ionic transport number, the fundamental conductivity relationship was used:

$$\sigma_{total} = \sigma_{ionic} + \sigma_{electronic} \text{ ----------(8)}$$

The analysis of the time-dependent conductivity behaviour revealed an exceptionally high ionic transport number exceeding 0.999 for the x = 0.05 specimen.

This remarkably high ionic transport number described that electrical conduction in this ceramic material occurs almost exclusively through the movement of lithium ions, with negligible electronic contribution. Such predominant ionic conductivity is a critical requirement for solid electrolyte applications in advanced battery technologies, as it prevents internal short-circuiting while enabling efficient ion transfer between electrodes. The results validate the effectiveness of the compositional engineering approach in developing highly ion-conductive garnet-type solid electrolytes with minimal electronic conductivity.

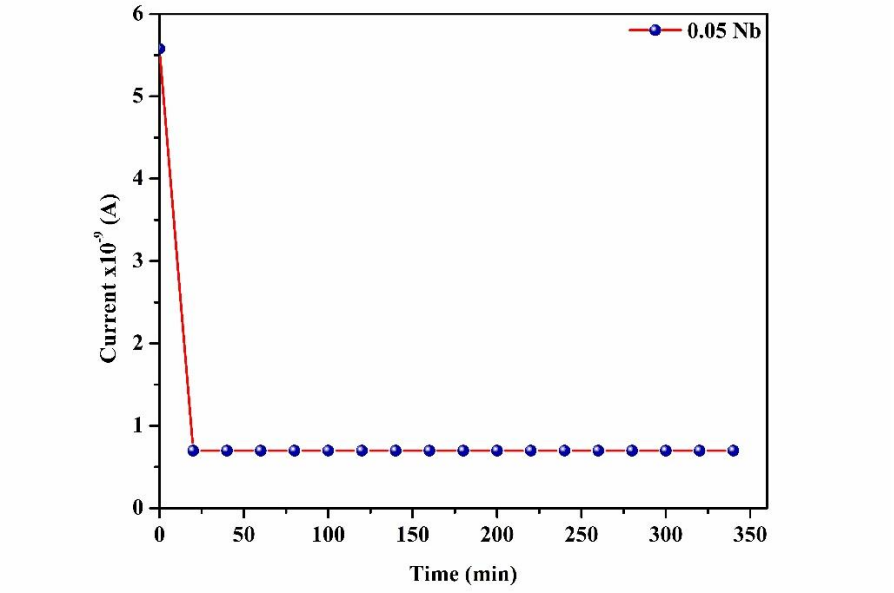

Figure 18: Variation of DC conductivity with time for $Li_{6.4}Ga_{0.20}La_{2.95}Sr_{0.05}Zr_{1.95}Nb_{0.05}O_{12}$.

CHAPTER 5
CONCLUSIONS

This study delves into the intricate properties of lithium ion conducting garnet-type ceramic solid electrolytes (LLZO) through the investigation and synthesis of Ga, Sr and Nb doped LLZO. The comprehensive understanding is achieved thorough employing X ray diffraction (XRD), density measurements, scanning electron microscopy (SEM), and Electrical conductivity measurements. From the present research work, the following points can be inferred:

5.1 For pure LLZO

1. The LLZO synthesized using the solid state reaction method exhibited a cubic crystal structure, as confirmed by X-ray diffraction analysis. However, some shoulder peaks in the XRD pattern indicated the presence of a secondary $La_2Zr_2O_7$ pyrochlore phase.
2. Density measurements revealed that the pure LLZO sample had a bulk density of 4.32 g/cm³, corresponding to a relative density of approximately 84.7%.
3. Electrical conductivity measurements showed that the sample exhibited an ionic conductivity of 8.376×10^{-6} S/cm at RT.
4. The activation energy for lithium ion conduction was determined to be 0.61 eV.

5.2 For Ga, Sr and Nb Doped LLZO

1. The ceramic samples of series $Li_{6.45-x}Ga_{0.20}La_{2.95}Sr_{0.05}Zr_{2-x}Nb_xO_{12}$ were synthesized using solid state reaction method.
2. The series $Li_{6.45-x}Ga_{0.20}La_{2.95}Sr_{0.05}Zr_{2-x}Nb_xO_{12}$, with varying Nb content exhibits consistent trends in each characterization, aiding in the understanding of dopant behaviour.
3. Thorough X-ray diffraction (XRD) investigation of the samples revealed development of cubic phase for all compositions.

4. The highest density of 4.79 g/cm³ was achieved for $Li_{6.4}Ga_{0.20}La_{2.95}Sr_{0.05}Zr_{1.95}Nb_{0.05}O_{12}$ sintered at 1050 ℃ with corresponding relative density of approximately 95.78%, indicating optimal densification for this composition.
5. Scanning electron microscopy along with elemental mapping revealed uniform distribution of Ga^{3+}, Sr^{2+} and Nb^{5+} across the sample. Notably, the sample with x=0.05 a.p.f.u. exhibited larger grain size, further supporting the better sintering effect due to the dopants.
6. The maximum ionic conductivity of 2.92 $x10^{-4}Scm^{-1}$ at RT with minimum activation energy of 0.30 eV, was observed for $Li_{6.4}Ga_{0.20}La_{2.95}Sr_{0.05}Zr_{1.95}Nb_{0.05}O_{12}$ This conductivity marks a significant increase from the ionic conductivity of pure LLZO, which is 8.376 x 10^{-6} Scm^{-1}, achieved through the tri-doping of Ga (0.20), Sr (0.05) and Nb (0.05). However, beyond this point of optimum 0.05 Nb content, the ionic conductivity begins to decrease. The decrease in conductivity has been attributed to lowering of Li content as the Nb content increase beyond optimum limit.
7. Electrical conductivity measurements showed that the composition with x = 0.05 exhibited the highest ionic conductivity, correlating well with its maximum relative density.
8. The lowest activation energy was obtained for x = 0.05, aligning with the trends in conductivity.
9. Transport number measurements confirmed that the conductivity in these materials was predominantly ionic, with values exceeding 0.999, ruling out electronic contribution.

In conclusion, substituting Ga at Li, Sr at La and Nb at Zr in the LLZO structure enhanced lithium-ion conductivity by increasing the concentration of lithium vacancies and creating more efficient migration pathways. This also contributed to reduced activation energy and improved overall performance of the solid electrolyte.

5.3 Scope for future work:

In spite of detailed work carried out, there is a scope for the future work as given below:

1. Improve ionic conductivity of Ga-Sr and Nb tri-doped LLZO by optimizing sintering temperature and time.

2. Explore substitution of other dopants to enhance ionic conductivity of LLZO.

3. Implement multi-doping techniques to further improve the ionic conductivity of LLZO.

4. Study the long-term stability of LLZO under various environmental conditions.

5.4 References

[1] A. J. P. K. D. K. S. T. Christine Jeyaseelan, *Ni-Cd Batteries*. 2020.

[2] M. S. Whittingham, "Lithium batteries and cathode materials," *Chem Rev*, vol. 104, no. 10, pp. 4271–4301, Oct. 2004, doi: 10.1021/cr020731c.

[3] J. B. Goodenough, "Electrochemical energy storage in a sustainable modern society," 2014, *Royal Society of Chemistry*. doi: 10.1039/c3ee42613k.

[4] B. Roling, J. Kettner, and V. Miß, "A General Classification of Electrolyte Solutions Based on Their Charge and Mass Transport Properties."

[5] Y. K. Liu, C. Z. Zhao, J. Du, X. Q. Zhang, A. B. Chen, and Q. Zhang, "Research Progresses of Liquid Electrolytes in Lithium-Ion Batteries," Feb. 22, 2023, *John Wiley and Sons Inc*. doi: 10.1002/smll.202205315.

[6] V. Thangadurai and W. Weppner, "Recent progress in solid oxide and lithium ion conducting electrolytes research," *Ionics (Kiel)*, vol. 12, no. 1, pp. 81–92, May 2006, doi: 10.1007/s11581-006-0013-7.

[7] Klaus Brandt, *Electrochemical Power Sources: Fundamentals, Systems, and Applicatios*. susan dennis, 2019.

[8] V. Thangadurai and W. Weppner, "Recent progress in solid oxide and lithium ion conducting electrolytes research," *Ionics (Kiel)*, vol. 12, no. 1, pp. 81–92, May 2006, doi: 10.1007/s11581-006-0013-7.

[9] J. Y. Song, Y. Y. Wang, and C. C. Wan, "Review of gel-type polymer electrolytes for lithium-ion batteries," 1999.

[10] P. M. J. N. Vashishta, *Fast ion transport in solids: electrodes and electrolytes*. Elsevier North Holland, Inc., 1979.

[11] J. Awaka, A. Takashima, K. Kataoka, N. Kijima, Y. Idemoto, and J. Akimoto, "Crystal structure of fast lithium-ion-conducting cubic Li 7La3Zr2O12," *Chem Lett*, vol. 40, no. 1, pp. 60–62, 2011, doi: 10.1246/cl.2011.60.

[12] M. M. Raju, F. Altayran, M. Johnson, D. Wang, and Q. Zhang, "Crystal Structure and Preparation of Li7La3Zr2O12 (LLZO) Solid-State Electrolyte and Doping Impacts on the Conductivity: An Overview," Sep. 01, 2021, *Multidisciplinary Digital Publishing Institute (MDPI)*. doi: 10.3390/electrochem2030026.

[13] S. Adams and R. P. Rao, "Ion transport and phase transition in Li 7-xLa 3(Zr 2-xM x)O 12 (M = Ta 5+, Nb 5+, x = 0, 0.25)," *J Mater Chem*, vol. 22, no. 4, pp. 1426–1434, Jan. 2012, doi: 10.1039/c1jm14588f.

[14] C. A. Geiger *et al.*, "Crystal chemistry and stability of 'Li7La 3Zr2O12' garnet: A fast lithium-ion conductor," *Inorg Chem*, vol. 50, no. 3, pp. 1089–1097, Feb. 2011, doi: 10.1021/ic101914e.

[15] T. Thompson *et al.*, “A tale of two sites: On defining the carrier concentration in Garnet-based ionic conductors for advanced Li batteries,” *Adv Energy Mater*, vol. 5, no. 11, Jun. 2015, doi: 10.1002/aenm.201500096.

[16] C. H. Lee *et al.*, “Low temperature synthesis of garnet type solid electrolyte by modified polymer complex process and its characterization,” *Mater Res Bull*, vol. 83, pp. 309–315, Nov. 2016, doi: 10.1016/j.materresbull.2016.02.040.

[17] E. Rangasamy, J. Wolfenstine, J. Allen, and J. Sakamoto, “The effect of 24c-site (A) cation substitution on the tetragonal-cubic phase transition in Li7-xLa3-xAxZr 2O12 garnet-based ceramic electrolyte,” *J Power Sources*, vol. 230, pp. 261–266, 2013, doi: 10.1016/j.jpowsour.2012.12.076.

[18] I. Kokal, M. Somer, P. H. L. Notten, and H. T. Hintzen, “Sol-gel synthesis and lithium ion conductivity of Li7La 3Zr2O12 with garnet-related type structure,” *Solid State Ion*, vol. 185, no. 1, pp. 42–46, Mar. 2011, doi: 10.1016/j.ssi.2011.01.002.

[19] S. Kumazaki *et al.*, “High lithium ion conductive Li7La3Zr 2O12 by inclusion of both Al and Si,” *Electrochem commun*, vol. 13, no. 5, pp. 509–512, May 2011, doi: 10.1016/j.elecom.2011.02.035.

[20] J. Tan and A. Tiwari, “Fabrication and characterization of Li7La3Zr 2O12 thin films for lithium ion battery,” *ECS Solid State Letters*, vol. 1, no. 6, 2012, doi: 10.1149/2.013206ssl.

[21] S. Kim, M. Hirayama, S. Taminato, and R. Kanno, “Epitaxial growth and lithium ion conductivity of lithium-oxide garnet for an all solid-state battery electrolyte,” *Dalton Transactions*, vol. 42, no. 36, pp. 13112–13117, Sep. 2013, doi: 10.1039/c3dt51795k.

[22] Y. Shimonishi *et al.*, “Synthesis of garnet-type Li7 - XLa3Zr 2O12 - 1/2x and its stability in aqueous solutions,” *Solid State Ion*, vol. 183, no. 1, pp. 48–53, Feb. 2011, doi: 10.1016/j.ssi.2010.12.010.

[23] D. J. Kalita, S. H. Lee, K. S. Lee, D. H. Ko, and Y. S. Yoon, “Ionic conductivity properties of amorphous Li-La-Zr-O solid electrolyte for thin film batteries,” *Solid State Ion*, vol. 229, pp. 14–19, Dec. 2012, doi: 10.1016/j.ssi.2012.09.011.

[24] J. Tan and A. Tiwari, “Fabrication and characterization of Li7La3Zr 2O12 thin films for lithium ion battery,” *ECS Solid State Letters*, vol. 1, no. 6, 2012, doi: 10.1149/2.013206ssl.

[25] J. F. Wu *et al.*, “Gallium-doped Li7La3Zr2O12 garnet-type electrolytes with high lithium-ion conductivity,” *ACS Appl Mater Interfaces*, vol. 9, no. 2, pp. 1542–1552, Jan. 2017, doi: 10.1021/acsami.6b13902.

[26] J. Sakamoto, E. Rangasamy, H. Kim, Y. Kim, and J. Wolfenstine, “Synthesis of nano-scale fast ion conducting cubic Li7La 3Zr2O12,” *Nanotechnology*, vol. 24, no. 42, Oct. 2013, doi: 10.1088/0957-4484/24/42/424005.

[27] D. Rettenwander *et al.*, “Interface instability of fe-stabilized Li7La3Zr2O12 versus li metal,” *Journal of Physical Chemistry C*, vol. 122, no. 7, pp. 3780–3785, Feb. 2018, doi: 10.1021/acs.jpcc.7b12387.

[28] S. Ohta, T. Kobayashi, and T. Asaoka, “High lithium ionic conductivity in the garnet-type oxide Li7-X La3(Zr2-X, NbX)O12 (X = 0-2),” *J Power Sources*, vol. 196, no. 6, pp. 3342–3345, Mar. 2011, doi: 10.1016/j.jpowsour.2010.11.089.

[29] J. Y. Song, Y. Y. Wang, and C. C. Wan, “Review of gel-type polymer electrolytes for lithium-ion batteries,” 1999.

[30] Y. Li *et al.*, “W-Doped Li7La3Zr2O12 Ceramic Electrolytes for Solid State Li-ion Batteries,” *Electrochim Acta*, vol. 180, pp. 37–42, Oct. 2015, doi: 10.1016/j.electacta.2015.08.046.

[31] C. Deviannapoorani, S. Ramakumar, N. Janani, and R. Murugan, “Synthesis of lithium garnets from La2Zr2O7 pyrochlore,” *Solid State Ion*, vol. 283, pp. 123–130, Dec. 2015, doi: 10.1016/j.ssi.2015.10.006.

[32] M. Aote and A. V. Deshpande, “Study of Ge-doped garnet type Li7La3Zr2O12 as solid electrolyte for Li-ion battery application,” *Journal of Materials Science: Materials in Electronics*, vol. 35, no. 8, Mar. 2024, doi: 10.1007/s10854-024-12338-5.

[33] D. Rettenwander *et al.*, “Structural and Electrochemical Consequences of Al and Ga Cosubstitution in Li7La3Zr2O12 Solid Electrolytes,” *Chemistry of Materials*, vol. 28, no. 7, pp. 2384–2392, Apr. 2016, doi: 10.1021/acs.chemmater.6b00579.

[34] S. Narayanan, F. Ramezanipour, and V. Thangadurai, “Enhancing Li ion conductivity of garnet-type Li 5La 3Nb 2O 12 by Y- and Li-codoping: Synthesis, structure, chemical stability, and transport properties,” *Journal of Physical Chemistry C*, vol. 116, no. 38, pp. 20154–20162, Sep. 2012, doi: 10.1021/jp304737x.

[35] L. Dhivya and R. Murugan, “Effect of simultaneous substitution of y and Ta on the stabilization of cubic phase, microstructure, and Li+ conductivity of Li7La3Zr2O12 lithium garnet,” *ACS Appl Mater Interfaces*, vol. 6, no. 20, pp. 17606–17615, Oct. 2014, doi: 10.1021/am503731h.

[36] R. Murugan, V. Thangadurai, and W. Weppner, “Effect of lithium ion content on the lithium ion conductivity of the garnet-like structure Li5+xBaLa2Ta2O 11.5+0.5x (x = 0-2),” *Appl Phys A Mater Sci Process*, vol. 91, no. 4, pp. 615–620, Jun. 2008, doi: 10.1007/s00339-008-4494-2.

[37] W. G. Zeier, S. Zhou, B. Lopez-Bermudez, K. Page, and B. C. Melot, “Dependence of the li-ion conductivity and activation energies on the crystal structure and ionic radii in Li6MLa2Ta 2O12,” Jul. 23, 2014, *American Chemical Society*. doi: 10.1021/am4060194.

[38] M. Aote, A. V. Deshpande, A. Khapekar, and K. Parchake, “Influence of Ga-Ge doping on the structural and electrical properties of Li7La3Zr2O12 solid electrolytes,” *Mater Lett*, vol. 377, Dec. 2024, doi: 10.1016/j.matlet.2024.137462.

[39] M. Aote and A. V. Deshpande, “Enhancement in Li-ion conductivity through Co-doping of Ge and Ta in garnet Li7La3Zr2O12 solid electrolyte,” *Ceram Int*, vol. 49, no. 24, pp. 40011–40018, Dec. 2023, doi: 10.1016/j.ceramint.2023.09.330.

[40] M. Kim, G. Kim, and H. Lee, “Tri-doping of sol–gel synthesized garnet-type oxide solid-state electrolyte,” *Micromachines (Basel)*, vol. 12, no. 2, pp. 1–14, 2021, doi: 10.3390/mi12020134.

[41] Y. Meesala *et al.*, “An efficient multi-doping strategy to enhance Li-ion conductivity in the garnet-type solid electrolyte Li7La3Zr2O12,” *J Mater Chem A Mater*, vol. 7, no. 14, pp. 8589–8601, 2019, doi: 10.1039/c9ta00417c.

[42] Y. Meesala *et al.*, “An efficient multi-doping strategy to enhance Li-ion conductivity in the garnet-type solid electrolyte Li7La3Zr2O12,” *J Mater Chem A Mater*, vol. 7, no. 14, pp. 8589–8601, 2019, doi: 10.1039/c9ta00417c.

[43] M. Aote and A. V. Deshpande, “Study of Ge-doped garnet type Li7La3Zr2O12 as solid electrolyte for Li-ion battery application,” *Journal of Materials Science: Materials in Electronics*, vol. 35, no. 8, Mar. 2024, doi: 10.1007/s10854-024-12338-5.

[44] N. Birkner, C. Li, S. L. Estes, and K. S. Brinkman, “Gallium-Doping Effects on Structure, Lithium-Conduction, and Thermochemical Stability of Li7-3xGaxLa3Zr2O12 Garnet-Type Electrolytes,” *ChemSusChem*, vol. 14, no. 12, pp. 2621–2630, Jun. 2021, doi: 10.1002/cssc.202100526.

[45] C. Chen *et al.*, “Microstructural and Electrochemical Properties of Al- And Ga-Doped Li7La3Zr2O12 Garnet Solid Electrolytes,” *ACS Appl Energy Mater*, vol. 3, no. 5, pp. 4708–4719, May 2020, doi: 10.1021/acsaem.0c00347.